ELSEVIER

Contents lists available at ScienceDirect

# Geochimica et Cosmochimica Acta

journal homepage: www.elsevier.com/locate/gca





# Clumped and conventional isotopes of natural gas reveal basin burial, denudation, and biodegradation history

Ji-Hyun Kim $^{a,b,c,*}$ , Anna M. Martini $^d$ , Shuhei Ono $^e$ , Ellen Lalk $^{e,f,g}$ , Grant Ferguson $^{a,h}$ , Jennifer C. McIntosh $^{a,h}$ 

- <sup>a</sup> Department of Hydrology and Atmospheric Sciences, The University of Arizona, Tucson, AZ, USA
- <sup>b</sup> Department of Geoscience, University of Calgary, Calgary, Alberta, Canada
- <sup>c</sup> Korea Institute of Geoscience and Mineral Resources, Daejeon, Republic of Korea
- <sup>d</sup> Department of Geology and Environmental Studies, Amherst College, Amherst, MA, USA
- <sup>e</sup> Department of Earth, Atmospheric, and Planetary Sciences, Massachusetts Institute of Technology, Cambridge, MA, USA
- f MIT-WHOI Joint Program in Oceanography/Applied Ocean Science and Engineering, Cambridge and Woods Hole, MA, USA
- g United States Geological Survey, Woods Hole, MA, USA
- h Department of Civil, Geological and Environmental Engineering, University of Saskatchewan, Saskatoon, Canada

#### ARTICLE INFO

#### Associate editor: Stefano M. Bernasconi

#### Keywords:

Clumped isotopologues of methane Thermal maturity of hydrocarbons Biodegradation of hydrocarbons Hydrogen isotope exchange

#### ABSTRACT

Formation and post-genetic alteration of hydrocarbons provide insights into the dynamic and complex geologic, hydrologic, and microbial history of shallow crustal environments. Clumped isotopologues of methane (e.g.,  $\Delta^{13}$ CH $_{3}$ D) have emerged as a proxy for constraining methane formation temperatures in sedimentary basins. However, unrealistically high apparent temperatures and microbial cycling of methane necessitate further investigation into how the generation and biodegradation of hydrocarbons may modify methane clumped isotopologue signatures. This study analyzed and modeled the clumped isotopologues of methane, in addition to traditional gas isotopes, to provide new insights into the origin, thermal maturity, migration, and biodegradation histories of hydrocarbons in the Paradox Basin in the Colorado Plateau. The basin was deeply buried in the geologic past and has been recently incised, leading to rapid denudation, enhanced meteoric circulation, and microbial activity.  $\delta^{13}C_{CH4}$  and  $CH_4/\Sigma C_{2+}$  ratios suggest that most natural gases in various reservoirs throughout the basin are thermogenic in origin with variable thermal maturities. However, signatures suggestive of anaerobic oxidation of ethane and propane, and secondary microbial methane generation, exist. In the northeastern part of the basin,  $\Delta^{13}CH_3D$  values in reservoirs above and below the Paradox Formation source rocks are consistent with thermodynamic equilibrium, indicating that the thermally mature hydrocarbons equilibrated at >160 °C during maximum burial over 30–80 Ma. Disequilibrium  $\Delta^{13}$ CH<sub>3</sub>D values of natural gas in Paradox Formation reservoirs along the southwestern margin of the basin suggest the presence of low-maturity hydrocarbons consistent with the region's shallower burial history. Models of  $\Delta^{13}$ CH<sub>3</sub>D values based on the exchange rate of hydrogen isotopes between methane and water and the basin thermal history support that meteoric recharge and microbial activity, following incision/denudation over the past few million years, promoted anaerobic oxidation of hydrocarbons (particularly ethane and propane), biodegradation of crude oil, and generation of secondary microbial methane in shallow reservoirs.

#### 1. Introduction

Understanding the evolution of hydrocarbons in sedimentary basins provides important insights into fluid generation and migration, and microbial activity (Martini et al., 1996; Head et al., 2003; Martini et al., 2008; Osborn and McIntosh, 2010). These processes are related to basin

burial and denudation history and play a key role in carbon cycling in the upper few kilometers of crust (Bose, et al., 2013; Schweitzer et al., 2019). Molecular (C<sub>1</sub>, C<sub>2</sub>, C<sub>3</sub>, etc.) and isotopic (i.e.,  $\delta^{13}$ C and  $\delta$ D) compositions of hydrocarbons have been widely used as tracers of the origin of natural gas and post-genetic physical and biologic processes (Bernard et al., 1976; Chung et al., 1988; Prinzhofer and Huc, 1995;

<sup>\*</sup> Corresponding author now at: Korea Institute of Geoscience and Mineral Resources, Daejeon, Republic of Korea. *E-mail address*: jihyun.kim@kigam.re.kr (J.-H. Kim).

Prinzhofer and Pernaton, 1997; Schoell, 1988; Whiticar, 1999). However, these 'traditional' isotopic approaches often yield overlapping or ambiguous signatures of thermogenic versus microbial methane and biodegradation of hydrocarbons (Vinson et al., 2017). New techniques, based on measurements of multiply substituted ('clumped') methane isotopologues (Ma et al., 2008; Tsuji et al., 2012; Stolper et al., 2014a, b; Ono et al., 2014) may provide a more quantitative proxy to constrain temperatures of methane formation although fractionation may complicate the interpretation (Stolper et al., 2015; Wang et al., 2015; Douglas et al., 2016, 2017).

While many laboratory studies (Stolper et al., 2014b; Wang et al., 2016; Shuai et al., 2018; Xia and Gao, 2019) and well-constrained thermogenic gas fields (Wang et al., 2015; Douglas et al., 2017; Giunta et al., 2019) have yielded isotopologue equilibrium temperatures commensurate with temperatures of formation, many other complex basin systems with microbial gas have yielded more ambiguous results (Stolper et al., 2014a; Giunta et al., 2019). Isotopologues for thermogenic methane in the Potiguar Basin in Brazil show methane formation at deeper depths with higher temperatures compared to current reservoir conditions and provide new insights into gas migration and mixing associated with thermal and burial history (Stolper et al., 2014a). Natural gas in the Devonian Antrim Shale of the Michigan Basin is generated dominantly through microbial methanogenesis (Martini et al., 1998; 2003); however, methane isotopologue signatures suggest the natural gas is predominantly thermogenic in origin (Giunta et al., 2019), provoking questions about post-genetic reprocessing of methane isotopologues. Furthermore, several natural gas samples have been reported with anomalous clumped isotope values indicating unrealistically high apparent temperatures (>300 °C) of thermogenic methane formation (Douglas et al., 2017; Stolper et al., 2018; Xie et al., 2021), suggestive of kinetically controlled reactions. More conclusive interpretations of methane isotopologues require an understanding of the complex hydrologic and geologic (e.g., burial, uplift, tectonic activity) history of basins inducing different thermal regimes, fluid flow, and biodegradation of hydrocarbons, during and after their generation.

Post-genetic biodegradation processes in oil and gas reservoirs include biodegradation of crude oil producing secondary microbial methane (Matyasik et al., 2000; Pallasser, 2000; Masterson et al., 2001; Jones et al., 2008), anaerobic oxidation of methane (Knittel and Boetius, 2009; Valentine, 2011), and/or anaerobic oxidation of other short-chain hydrocarbons (James and Burns, 1984; Wenger et al., 2002; Martini et al., 1998, 2003, and 2008; Adams et al., 2013; Bose et al., 2013). The effects of post-genetic biodegradation on molecular and isotopic composition of hydrocarbons in natural gas have been evaluated using conventional isotopic approaches (Wang et al., 2005; Tilley and Muehlenbachs, 2006; Vandré et al., 2007; Zhou et al., 2008; Zhi et al., 2021; Jautzy et al., 2021), while the effects of biodegradation on clumped isotopologue compositions are still poorly defined (Wang et al., 2015, 2016).

The Paradox Basin in the Colorado Plateau contains widespread oil and gas fields and a dynamic geologic and hydrologic history (Nuccio and Condon, 1996; Rasmussen and Rasmussen, 2009; Whidden et al., 2014), providing a natural laboratory to study the co-evolution of formation water, hydrocarbons, and microbial communities over geologic time. Pervasive bleached, former redbed sandstones (e.g., Jurassic Navajo Sandstone) and residual bitumen provide evidence of large-scale (Beitler et al., 2003) hydrocarbon generation and expulsion during maximum burial, migration along faults into shallow sediments from the Pennsylvanian Paradox Formation source rocks, and subsequent postgenetic (microbial) alteration (Merin and Segal, 1989; Foxford et al., 1998; Chan et al., 2000; Thorson and MacIntyre, 2005; Hahn and Thorson, 2006; Hodson et al., 2016; Barton et al., 2018; Thorson, 2018; Kim et al., 2022a). Early-stage thermogenic gases may have also been post-genetically altered by high temperatures during maximum burial. Hydrocarbons may have been remobilized by topographically-driven groundwater flow and expelled or biodegraded by rapid incision and

breaching of shallow reservoirs (Beitler et al., 2003) following recent denudation of Colorado Plateau (<4–10 Ma; Lazear et al., 2013; Murray et al., 2016, 2019). Meteoric circulation around salt walls in the Paradox Basin generated high SO<sub>4</sub> from gypsum dissolution, enhancing bacterial sulfate reduction (BSR) in the presence of organic-rich shales (Kim et al, 2022a). BSR may have also been coupled with the anaerobic oxidation of hydrocarbons in reservoirs proximal to salt walls, as seen in previous studies of other environments, for example, ethane degradation coupled to BSR in sediments from hydrothermal vents (Adams et al., 2013), and BSR-coupled oxidation of alkanes, including methane, in marine hydrocarbon seeps (Bose et al., 2013). On the other hand, microbial methane, mixed with thermogenic gases, is present in Cretaceous coalbeds in east-central Utah (Mancos Shale/Ferron Sandstone; Rice, 2003) and Dakota Sandstone oil reservoirs in the Uinta Basin (Zhang et al. 2009), proximal to the Paradox Basin.

To better constrain the prolonged history of hydrocarbon generation and post-genetic (e.g., thermal and microbial) alterations in the Paradox Basin, we link the geological (e.g., erosion and incision) and hydrological (e.g., meteoric water circulation) history of the basin to natural gas geochemistry ( $\delta^{13}C$ ,  $\delta D$ ,  $CH_4/\Sigma C_{2+}$ , and  $\Delta^{13}CH_3D$ ). We also evaluate the thermal equilibration of  $\Delta^{13}CH_3D$  values using the rate of isotopologue exchange and thermal history of different parts of the basin. Results from this study extend the range of previously reported  $\Delta^{13}CH_3D$  values and provide new insights into methane clumped isotopologues.

# 2. Study area

The Paradox Basin is located in southeastern Utah and southwestern Colorado, USA (Fig. 1A) within the Colorado Plateau. The basin is underlain by Precambrian basement rocks and was developed as a northeastward-deepening flexural basin in response to crustal loading by reverse faulting that generated the Late Paleozoic Uncompangre uplift of the ancestral Rocky Mountains (Baars and Stevenson, 1982; Barbeau, 2003; Leary et al., 2017). The Late Devonian Elbert Formation, including the basal McCracken Sandstone member and a dolomite and shale upper member, was deposited in a shallow marine environment (Fig. 1B; McBride, 2016). Renewed transgression in the Mississippian initiated deposition of the Leadville Limestone (Fig. 1B; Nuccio and Condon, 1996). Subsidence along the northeastern side of the Paradox Basin and marine transgressions during the Pennsylvanian led to cyclical deposition of marine evaporites and interbedded black shales, forming the thick (1.8 km where the salt is not severely disturbed) Paradox Formation (Baars, 1966; Hite et al., 1984; Nuccio and Condon, 1996; Rasmussen and Rasmussen, 2009). In the southwestern part of the basin (e.g., Greater Aneth field), the Paradox Formation is dominated by shelf carbonates, including algal-mound buildups (Nuccio and Condon, 1996). The black shale interbeds of the Ismay and Desert Creek members (interval) of the Upper Paradox Formation and the Cane Creek shale member of the Middle Paradox Formation are major hydrocarbon source rocks (Figs. 1B, 2A, and 2B). The black shales contain up to 11-20% total organic carbon of a combination of Type II and Type III kerogen (Nuccio and Condon, 1996; Rasmussen and Rasmussen, 2009; Whidden et al. 2014). The amount of Type III kerogen, which is typically terrestrial organic matter, increases eastward toward the ancestral Uncompangre Uplift (Nuccio and Condon, 1996).

Above the Paradox Formation, the Pennsylvanian Lower Honaker Trail Formation consists of limestone, sandstone, and shale deposited in a cyclic pattern from evaporitic to normal marine conditions. The Upper Honaker Trail Formation and overlying Permian Cutler Group are composed of arkosic sandstone sourced from erosion of the Uncompahgre Uplift. Triassic and Jurassic formations are composed of eolian and fluvial sediments with volcanic ash (Fig. 1B). The early Cretaceous sediments are composed of conglomeratic sandstone and mudstone (Nuccio and Condon, 1996), while the Upper Cretaceous Mancos Shale was deposited in the Western Interior Cretaceous seaway (Fig. 1B). Intrusion of laccoliths during the Paleogene and Neogene (28  $\pm$  1 Ma)

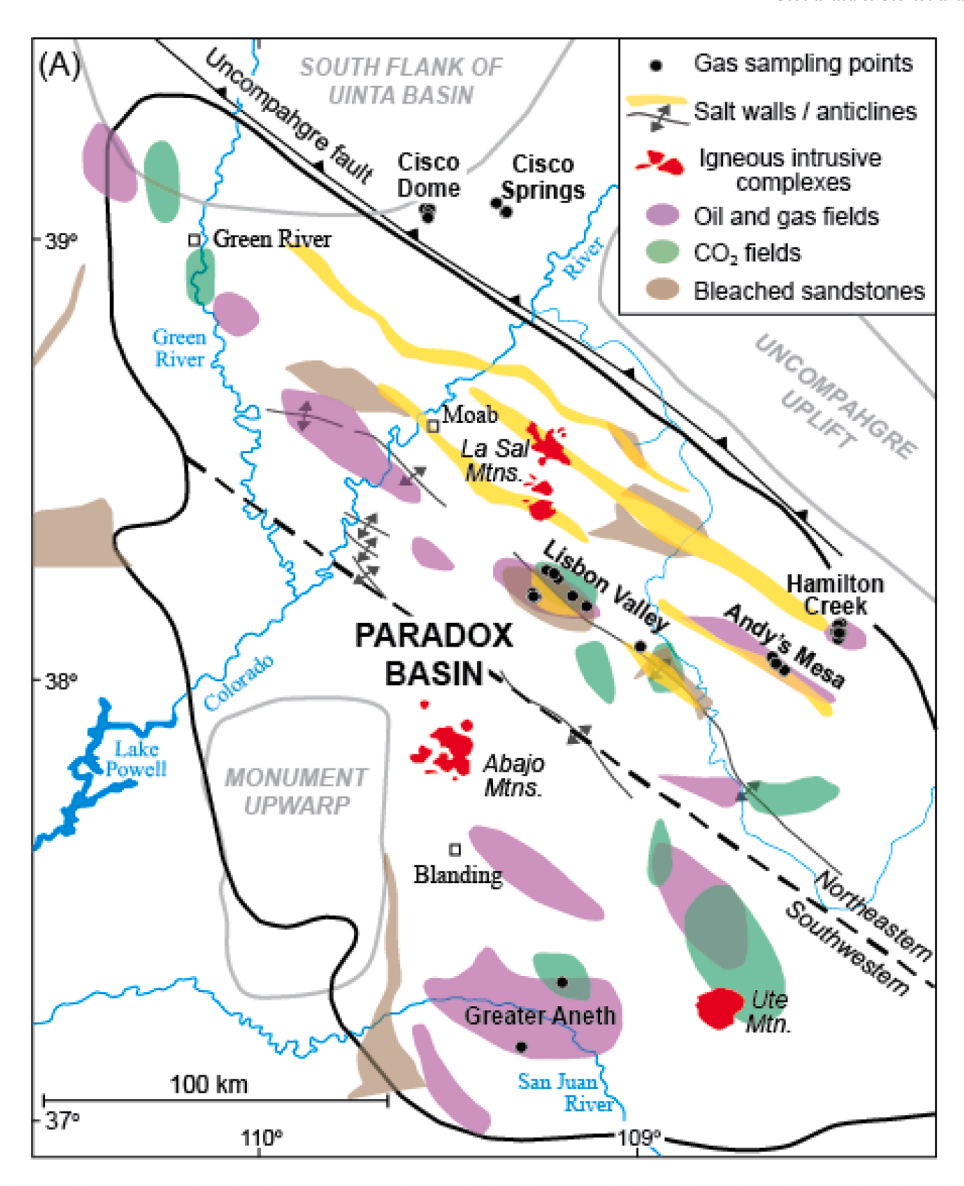


Fig. 1. (A) Location of the Paradox Basin, Colorado Plateau, USA, and spatial distributions of salt walls and anticlines, oil and gas fields,  $CO_2$  fields, bleached sandstones, modified from Barton et al. (2018). Dashed line represents the basin extent. (B) Stratigraphic column of Devonian through Cretaceous formations with vertical distribution of bleached sandstones, organic carbon sources, and oil and gas reservoirs in different fields where gas samples were collected. Different sample symbols are shown in brackets. Vitrinite reflectance ( $R_0$ ) values and corresponding oil and gas windows of the Upper and Middle Paradox Formation source rocks in northeastern/southwestern side of the Paradox Basin (Rasmussen and Rasmussen, 2009).

formed the La Sal, Abajo, and Ute mountains in the Paradox Basin (Fig. 1A; Nuccio and Condon, 1996; Friedman and Huffman, 1998; Barton et al., 2018; Murray et al., 2019).

Thick deposition of Permian through Neogene sediments led to plastic flow of the underlying Paradox Formation evaporites and created the salt walls/anticlines, associated faults (Hartley and Evenstar, 2018), and sub-basins along the northeastern side of the basin, for example in the Lisbon Valley areas (Cater and Craig, 1970; Doelling et al., 1988; Lawton et al., 2015; Nuccio and Condon, 1996; Trudgill, 2011). During the late Miocene, incision of the Colorado River and rapid denudation of the Colorado Plateau (<4–6 Ma, Murray et al., 2016 and 2019; <10 Ma, Lazear et al., 2013) removed most of the Cretaceous and overlying sediments (e.g., Mancos Shale confining units) (Nuccio and Condon, 1996), created relatively high topographic gradients (Karlstrom et al., 2012; Lazear et al., 2013; Pederson et al., 2013), and brought deep geologic formations and their fluids closer to the surface. The high topographic gradients allowed widespread paleofluid flow events resulting in ore mineralization (Bailey et al., 2022a and 2022b) and deep

meteoric circulation that flushed residual saline fluids from aquifers above and below the evaporite units and regenerated salinity and high  $SO_4$  concentrations via dissolution of halite and gypsum (Kim et al., 2022a).

The Pennsylvanian Paradox Formation and overlying Lower Honaker Trail Formation comprise the middle hydrostratigraphic unit – a regional confining unit (Thackston et al., 1981; Hanshaw and Hill, 1969). Regional groundwater flow in the Pennsylvanian Upper Honaker Trail Formation through Cretaceous formations above the evaporites is mainly controlled by topography (the upper hydrostratigraphic unit) with recharge around salt anticlines, uplifts, and mountains (Hanshaw and Hill, 1969; King et al., 2014; Thackston et al., 1981). Mississippian through Devonian formations are considered as a single, lower hydrostratigraphic unit with a regionally extensive flow system toward the southwest, as well as with a locally recharged flow system around laccoliths, such as the Abajo and La Sal Mountains (Nuccio and Condon, 1996; Barton et al., 2018) or along the margins of the salt anticlines (Hanshaw and Hill, 1969; Thackston et al., 1981).

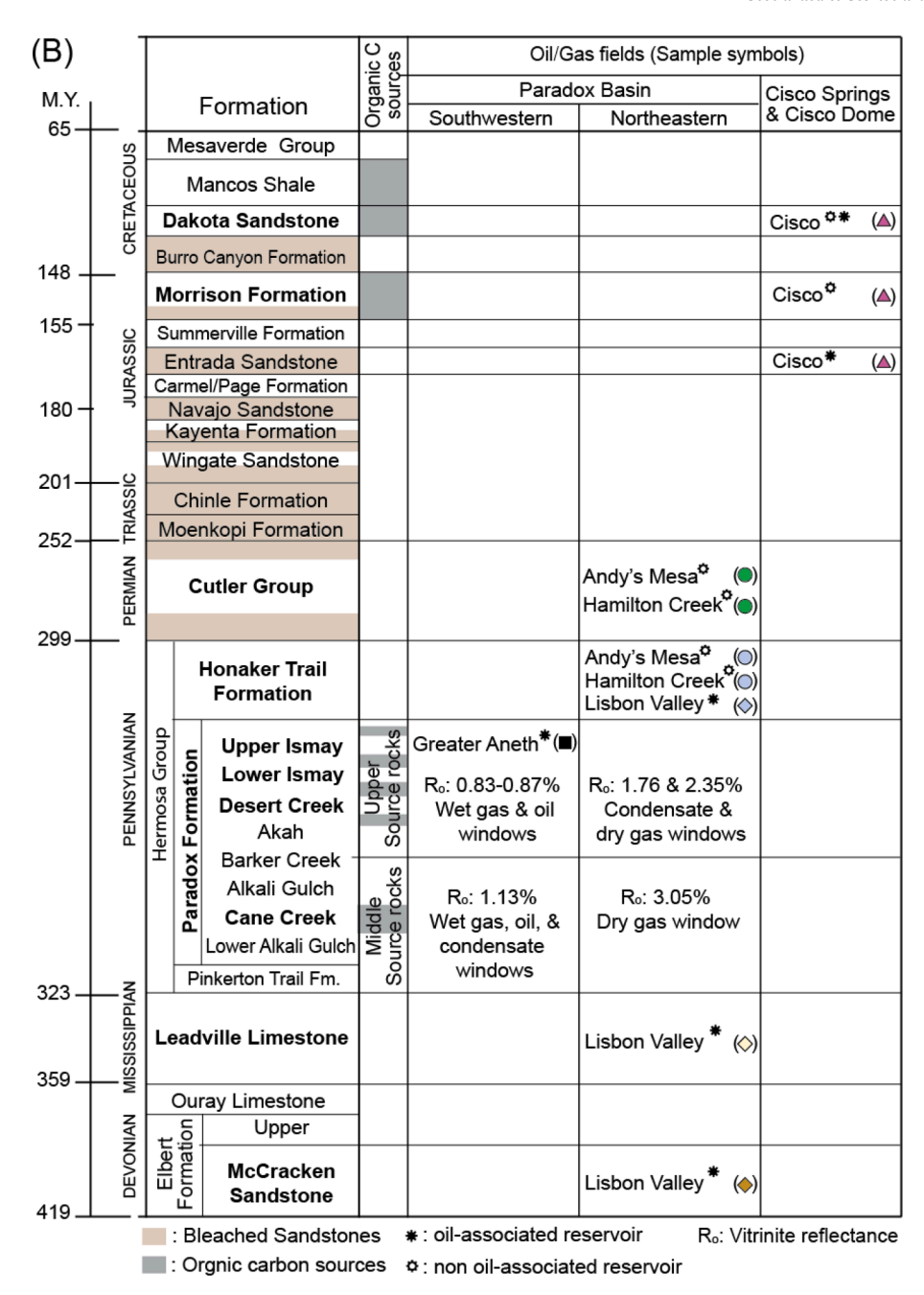
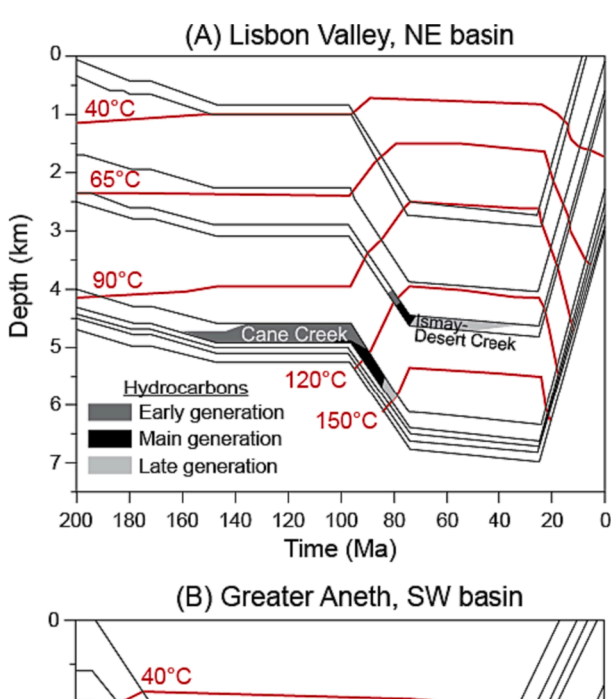
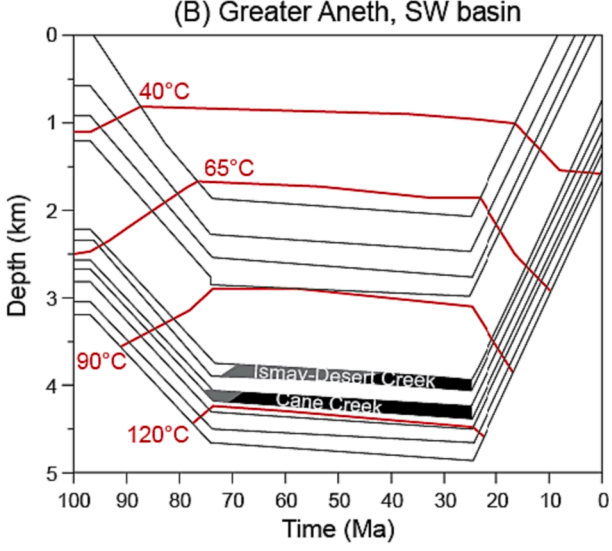
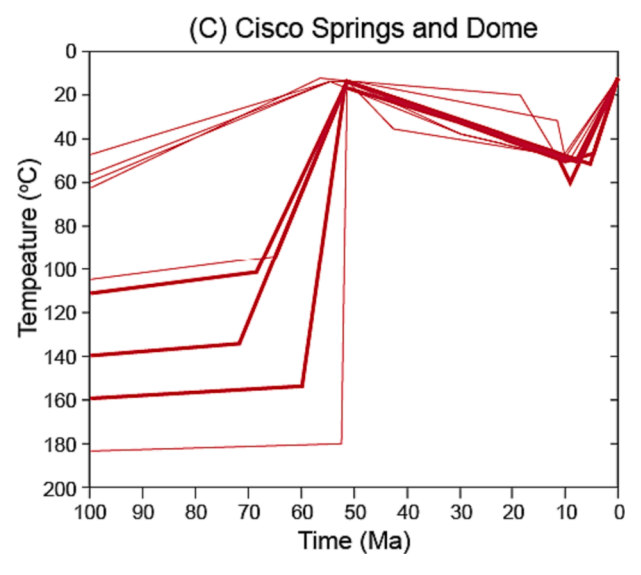


Fig. 1. (continued).

The relatively thick sedimentary sequence in the northeastern part of basin proximal to the Uncompangre Uplift (e.g., Lisbon Valley and Andy's Mesa fields; Fig. 1A) resulted in deeper burial and higher thermal maturities of the Cane Creek source rocks in the Paradox Formation (Figs. 1B and 2A), compared to the south-central and southwestern parts of the basin (e.g., Greater Aneth field; Figs. 1B and 2B) (Nuccio and Condon, 1996; Rasmussen and Rasmussen, 2009). For example, in the Lisbon Valley, early generation of hydrocarbons in the Cane Creek source rocks of the Middle Paradox Formation began as early as ~156 Ma. Significant generation of hydrocarbons occurred ~84-100 Ma and continued until the source rocks reached a maximum burial depth of 6.6 km~25 Ma (Fig. 2A; Nuccio and Condon, 1996). Thermal maturities of the Cane Creek source rocks in the northeastern part of the basin are relatively high (3.05% R<sub>o</sub>, vitrinite reflectance) within the dry gas window with ≥90% of transformation of kerogen (Fig. 1B; Rasmussen and Rasmussen, 2009). On the other hand, in the southwestern part of the Paradox Basin, the Ismay-Desert Creek source rocks began early generation of hydrocarbons ~74 Ma, started significant generation ~45 Ma, and were buried at a maximum depth of 4.1 km~25 Ma (Fig. 2B; Nuccio and Condon, 1996). Current thermal maturities of the Ismay-Desert Creek source rocks in the southwestern part of the basin range from 0.87 to 0.83% R<sub>0</sub>, within the wet gas and oil window with 46–54% transformation of kerogen (Fig. 1B; Rasmussen and Rasmussen, 2009). Significant oil and gas generation across the basin led to two peak upward and lateral fluid (i.e., water, oil, and gas) migration events around 66-100 Ma and 255-275 Ma (Lucero et al., 2020). Fluids generated within the source rocks likely migrated laterally within the Paradox Formation and vertically upwards along salt wall-bounding faults, especially in the northeastern part of the basin, and formed shallow reservoirs, for example in the overlying Honaker Trail Formation and Cutler Group in the Lisbon Valley, Andy's Mesa, and Hamilton Creek fields. Generation and primary migration of oil and gas from the Paradox







**Fig. 2.** Burial, thermal, and hydrocarbon generation history of (A) the Lisbon Valley field in the northeastern side of the Paradox Basin, (B) Greater Aneth field near the Monument upwarp are in the southwestern side of the basin (modified from Nuccio and Condon, 1996), and (C) Cisco Springs and Dome field near the Hay Canyon area of Book Cliffs (modified from Hoffman, 2009).

Formation ceased near the end of the Miocene, as the basin was incised, eroded, and cooled, beginning <10 Ma (Lazear et al., 2013) or <4–6 Ma (Murray et al., 2016; Murray et al., 2019).

The Cisco Springs and Cisco Dome fields (hereafter 'Cisco field') are located between the northeastern part of the Paradox Basin and the southern flank of the Uinta Basin (Fig. 1A), bounded to the north by the Mancos Shale outcrops in the Book Cliffs (Walton, 1956). The Cisco field lies upon north-west trending anticlines, which are a northern extension of the Uncompangre Uplift (Walton, 1956; Hendel, 1961), that were formed by post-Cretaceous uplift of the upthrown block of the Uncompahgre fault (Young, 1983). In this region, Jurassic sediments unconformably overlie Precambrian rocks of the Uncompangre Uplift (Young, 1983; Smouse 1996). Oil and gas in the Cisco field are dominantly produced from the Cretaceous Dakota Sandstone, with some production from the Jurassic Morrison and Entrada formations (Young, 1983) (Fig. 1). Different source rocks for hydrocarbons in the Cisco field have been hypothesized, including black shales in the Paradox Formation (Young, 1983) and/or organic-rich carbonaceous materials within the Morrison Formation, Dakota Sandstone, and/or overlying Mancos Shale (Hendel, 1961). The Mancos Shale and underlying sediments (e.g., Dakota Sandstone) reached ~110 to 190 °C during maximum burial ~100 Ma and experienced two rapid uplift/denudation events around 50-70 Ma and 10 Ma (Fig. 2C) (Hoffman, 2009), bringing the reservoirs closer to the surface under cooler conditions (20–60  $^{\circ}$ C) conducive for microbial degradation of hydrocarbons (McIntosh et al., 2023).

#### 3. Methods

Thirty-three natural gas samples were collected from active oil and gas wells (Fig. 1A and 1B) producing from the: 1) Mississippian Leadville Limestone and/or Devonian McCracken Sandstone in the Lisbon Valley field; 2) Pennsylvanian Paradox Formation (Ismay-Desert Creek members) in the Greater Aneth field; 3) Pennsylvanian Honaker Trail Formation in the Lisbon Valley field; 4) Pennsylvanian Honaker Trail Formation or Permian Cutler Group in the Andy's Mesa and Hamilton Creek fields; and 5) Cretaceous Dakota Sandstone and Jurassic Morrison (and Entrada) formations in the Cisco field (Fig. 1B and Table 1). Natural gas samples were collected in duplicate at the wellheads using a gas sampling manifold and Isotubes provided by Isotech Laboratories according to their instructions.

Natural gas samples were analyzed at Isotech Laboratories for gas composition and  $\delta^{13}$ C and  $\delta D$  values of methane (CH<sub>4</sub>) and higher chain hydrocarbons ( $C_2$ - $C_5$ ). Molecular and isotopic ( $\delta^{13}$ C) compositions of CO<sub>2</sub> were also analyzed at Isotech Laboratories. Gas molecular composition (He, H<sub>2</sub>, Ar, O<sub>2</sub>, CO<sub>2</sub>, N<sub>2</sub>, CO, CH<sub>4</sub>, and C<sub>2</sub>-C<sub>5</sub>) was determined on a Shimadzu 2010 Gas Chromatograph equipped with thermal conductivity and flame ionization detectors. The  $\delta^{13}C$  and  $\delta D$  values of hydrocarbons for most of the gas samples and  $\delta^{13}C$  values of  $CO_2$  were determined by conventional offline methods consisting of chromatographic separation followed by combustion and dual-inlet isotope ratio mass spectrometry with a precision of  $\pm 0.1\%$  for  $\delta^{13}$ C and  $\pm 2.0\%$  for δD. δD values of ethane and propane and/or n-butane of eleven samples (asterisk marked in Table 2) were measured online via compoundspecific analysis with gas chromatography combustion/pyrolysis isotope ratio mass spectrometry (GC-C/P-IRMS) (precision,  $\pm 0.3\%$  for  $\delta^{13}$ C and  $\pm 5.0\%$  for  $\delta D$ ) due to low concentrations. All gas component  $\delta^{13}\text{C}$  values are reported on a scale defined by a two-point calibration of LSVEC and NBS 19. Additional molecular and isotopic data from the Honaker Trail Formation (FF-4-20; MM36-14) from an unpublished dataset of Paradox Resources supplemented gas data for the Honaker Trail Formation (Tables 1 and 2).

Twenty-eight of the natural gas samples were also analyzed for the abundance of four isotopologues of methane ( $^{12}\text{CH}_4$ ,  $^{13}\text{CH}_4$ ), and  $^{13}\text{CH}_3\text{D}$ ) using Tunable Infrared Laser Direct Absorption Spectroscopy (TILDAS) at the Massachusetts Institute of Technology (Ono et al., 2014). Methane was purified using an automated preparative GC system

Geochimica et Cosmochimica Acta 361 (2023) 133–151

**Table 1**Sample location, depth, well type, and gas composition (mol%) of natural gases in the Paradox Basin.

Sample/well ID	Latitude	Longitude	Elevation (m)	Depth (m)	Field	Well	Formation	Не	H <sub>2</sub>	Ar	02	CO <sub>2</sub>	$N_2$	CO	CH <sub>4</sub>	$C_2$	$C_2H_4$	C <sub>3</sub>	C <sub>3</sub> H <sub>6</sub>	iC <sub>4</sub>	nC <sub>4</sub>	iC <sub>5</sub>	nC <sub>5</sub>	C <sub>6</sub> +	$CH_{4/}$ $\Sigma C_{2+}$
Federal1-355A	39.0826	-109.3714	1469	574	Cisco Springs	NAG	Dakota	0.2	nd	0.03	0.1	1.0	3	nd	87.8	4.2	nd	1.6	0.0001	0.7	0.5	0.4	0.2	0.5	14
Federal14-02	39.0623	-109.3443	1435	611	Cisco Springs	NAG	Dakota	0.1	nd	0.02	0.2	2.7	2	nd	88.9	4.3	nd	0.8	nd	0.4	0.1	0.1	0.02	0.3	17
Federal14-7	39.0685	-109.5616	1604	880	Cisco Dome	NAG	Dakota/Morrison	0.1	nd	0.01	0.03	3.5	2	nd	87.3	4.2	0.0003	1.3	0.0004	0.5	0.4	0.3	0.2	0.5	15
Federal13-2	39.0683	-109.5482	1602	785	Cisco Dome	NAG	Dakota/Morrison	0.1	0.5	0.01	0.04	1.9	1	nd	90.7	3.6	0.0002	0.8	0.0002	0.4	0.2	0.2	0.1	0.3	20
Federal24-2	39.0576	-109.5531	1593	884	Cisco Dome	NAG	Dakota/Morrison	0.2	nd	0.01	0.04	0.6	2	nd	94.0	2.6	0.0001	0.5	0.0002	0.2	0.1	0.1	0.04	0.1	29
TXO14-1	39.0616	-109.3485	1428	687	Cisco Springs	OAG	Dakota/Entrada	0.03	nd	0.01	0.2	4.3	1	nd	88.9	3.5	nd	0.6	0.0004	0.5	0.3	0.4	0.1	0.6	21
Federal31-1A		-109.5296		719	Cisco Dome	NAG	Dakota/Morrison	-	-	-	-	-	-	-	-	-	-	-	-	-	-	-	-	-	-
Union Gorit II-1	39.0503	-109.5532	1557	778	Cisco Dome	NAG	Morrison	0.1	nd	0.01	0.02	0.5	2	nd	93.8	2.7	0.0001	0.5	0.0002	0.2	0.1	0.1	0.03	0.2	29
AM-11	-	_	1993	1279	Andy's Mesa	NAG	Cutler	0.1	0.04	0.1	1.4	0.03	7	nd	88.3	2.1	0.001	0.5	0.0001	0.1	0.1	0.1	0.04	0.05	33
AM-38	38.0543	-108.6429	1950	1660	Andy's Mesa	NAG	Cutler	0.1	nd	0.2	4.4	0.1	19	nd	74.3	0.9	0.001	0.2	nd	0.1	0.1	0.04	0.03	0.1	61
AM-61	38.0245	-108.6112	2009	1705	Andy's Mesa	NAG	Cutler	0.2	nd	0.03	0.1	0.01	13	nd	83.7	2.0	0.001	0.2	nd	0.1	0.1	0.03	0.02	0.1	36
AM-62a	38.0245	-108.6112	1993	1711	Andy's Mesa	NAG	Cutler	0.2	0.1	0.1	0.9	0.03	17	nd	79.9	1.7	0.0003	0.1	nd	0.03	0.03	0.01	0.01	0.01	43
AM-62b	38.0245	-108.6112	2009	1711	Andy's Mesa	NAG	Cutler	0.2	0.02	0.03	0.1	0.01	14	nd	83.1	1.9	0.001	0.2	nd	0.03	0.1	0.02	0.02	0.05	38
HC-1-36	38.1109	-108.4749	2067	1255	Hamilton Creek	NAG	Cutler	0.4	0.04	0.04	0.05	0.02	18	nd	75.6	1.7	0.001	0.8	0.0004	0.6	0.8	0.6	0.5	0.7	23
AM-75a	38.0391	-108.6334	1958	2104	Andy's Mesa	NAG	Honaker Trail	0.1	0.04	0.03	0.6	0.03	6	nd	89.8	2.2	0.0002	0.5	nd	0.1	0.2	0.1	0.1	0.1	32
AM-75b	38.0391	-108.6334	1973.5	2208	Andy's Mesa	NAG	Honaker Trail	0.1	nd	0.01	0.1	0.1	5	nd	91.5	2.2	0.0003	0.5	nd	0.1	0.2	0.1	0.1	0.2	32
FF-4-20	-	_	_	-	Andy's Mesa	-	Honaker Trail	nd	nd	nd	0.1	0.03	6	nd	92.5	1.1	nd	0.3	na	0.1	0.1	0.1	0.05	0.2	65
FF-4-20	_	_	_	_	Andy's Mesa	_	Honaker Trail	nd	nd	nd	0.1	0.03	6	nd	92.3	1.1	nd	0.3	na	0.1	0.1	0.1	0.04	0.2	63
HC12-13	38.0946	-108.4685	2159	2280	Hamilton Creek	NAG	Honaker Trail	0.0	0.9	0.1	0.5	0.02	8	nd	87.3	1.3	0.0002	0.6	nd	0.3	0.4	0.3	0.1	0.3	38
HC-30-11	38.1296	-108.4611		2734	Hamilton Creek	NAG	Honaker Trail	0.1	0.01	0.01	0.04	0.7	4	nd	95.0	0.4	nd	0.04	nd	0.01	0.01	0.01	0.005	0.02	200
HC-25-22	38.1259	-108.4689	2008	1071	Hamilton Creek	NAG	Honaker Trail	0.1	0.01	0.01	0.1	0.6	4	nd	94.9	0.5	nd	0.1	nd	0.02	0.01	0.01	0.01	0.02	174
HC-36-23	38.1100	-108.4705	2084	2399	Hamilton Creek	NAG	Honaker Trail	0.05	nd	0.01	0.05	0.3	3	nd	95.3	1.0	nd	0.3	nd	0.1	0.1	0.1	0.0	0.1	71
HC-36-34	38.1079	-108.4661	2070	2326	Hamilton Creek	NAG	Honaker Trail	0.04	0.01	nd	0.04	0.4	2	nd	96.6	0.7	nd	0.1	nd	0.1	0.05	0.03	0.02	0.04	116
MM31-42	38 2319	-109.2099	2062	1617	Lisbon Valley	OAG	Honaker Trail	0.1	0.01	0.01	0.1	0.02	13	nd	69.2	9.5	0.001	4.1	0.0008	0.6	1.4	0.4	0.6	0.7	5
MM26-34		-109.2391		1617	Lisbon Valley		Honaker Trail	0.1	0.01	0.01				nd	69.9		0.002	4.8	0.002	0.7	1.5	0.4	0.5	0.4	4
MM36-14		-109.2207		2082	Lisbon Valley		Honaker Trail	0.14	na	na	na	0.03	8				na	4.0	na	0.5	1.1	0.3	0.3	0.6	5
BI24-31		-109.1340		947	Lisbon Valley		Honaker Trail	0.1		0.02		0.1	6	nd	93.2			0.0	nd	0.003					3204
BH10-31		-109.1719		1184	Lisbon Valley		Honaker Trail	0.0	nd	0.02		0.3	6		75.6		0.001	4.0	0.0017	0.7	1.1	0.002	0.003	0.02	
Sahgzie 1		-109.3064		1954	Greater Aneth		Paradox (Desert Creek)	0.0		0.02		0.1	2		51.3		nd	14	nd	2.6	6.8	2.3	2.3	2.1	
Monument-8n-	37.3163	-109.1979	1664	1895	Greater Aneth	OAG	Paradox (Desert Creek)	0.0	nd	0.05	1.3	0.1	3	nd	64.9	15	nd	8.5	nd	1.1	3.1	0.8	0.9	0.9	2
McIntyre 17-21	38.0772	-108.9913	1903	2586	Lisbon Valley	OAG	Leadville	0.8	0.1	0.1	0.7	7.1	13	nd	72.5	3.1	nd	1.4	nd	0.5	0.5	0.3	0.1	0.2	15
Lisbon B-610		-109.2771		2368	Lisbon Valley		Leadville	0.1	nd	0.02			4	nd			0.001	0.8	nd	0.1		0.04	0.05	0.1	6
Lisbon D8-10		-109.2771 $-109.2687$		2441	Lisbon Valley		Leadville/McCracken	0.5	0.5		0.04		11				nd	2.1	nd	0.3	0.13	0.04	0.03	0.1	3
Lisbon B8-10		-109.2687 $-109.2759$		2610	•		McCracken	0.5	0.03		0.05		16		59.0 59.0	12	nd nd	6.4	0.0002		2.1	0.2	0.2	0.2	3
Lisbon 10-33a		-109.2759 $-109.2737$		2610	Lisbon Valley		McCracken McCracken	0.5	nd	0.05	1.4	3.0					na nd			1.0	2.1 1.9	0.5	0.5	0.3	3
					Lisbon Valley													6.4	nd		2.43				
Lisbon 10-33b	38.1915	-109.2736	19/2	2702	Lisbon Valley	UAG	McCracken	0.3	nd	0.04	0.04	4.4	10	na	59.7	14	nd	7.5	nd	1.13	2.43	0.6	0.6	0.3	3

Abbreviations: NAG - Non-Associated Gas; OAG - Oil-associated Gas; nd - non-detected; na - not-analyzed.

**Table 2**Gas compound specific isotopic compositions of natural gases in the Paradox Basin.

Sample/well ID	δ <sup>13</sup> C <sub>CO2</sub> (‰)	δD <sub>H2O</sub> (‰)	δ <sup>13</sup> C <sub>CH4</sub> (‰)	δD <sub>CH4</sub> (‰)	δ <sup>13</sup> C <sub>C2</sub> (‰)	δD <sub>C2</sub> (‰)	δ <sup>13</sup> C <sub>C3</sub> (‰)	δD <sub>C3</sub> (‰)	δ <sup>13</sup> C <sub>nC4</sub> (‰)	Δ <sup>13</sup> CH <sub>3</sub> D (‰)	$2\sigma^2$ (‰)	<i>T</i> <sub>13D</sub> (°C)	+ (°C)	_ (°C)
Dakota/Morri	ison [Cisco f	ield1												-
Federal1- 355A	20.4	na	-44.0	-240.6	-27.2	-151.7	-22.1	-124.2	-23.4	3.5	0.3	129	17	15
Federal14- 02	22.5	-66.2	-46.0	-229.5	-25.5	-150.9	-20.2	-107.0	-22.2*	3.5	0.3	127	16	15
Federal14-7	19.0	-61.5	-42.2	-230.2	-26.7	-152.1	-24.2	-130.0	-25.9	3.0	0.3	162	25	23
Federal13-2	14.7	na	-42.3	-223.9	-26.4	-154.5	-21.2	-113.3	-24.1	3.6	0.5	121	34	28
Federal24-2	15.7	na	-41.9	-224.8	-26.5	-151.8	-23.0	-125.5	-25.3	3.3	0.3	140	18	16
TXO14-1	14.1	-61.8	-50.6	-242.8	-23.6	-134.8	-18.8*	-103.0 *	-22.9	4.5	0.2	76	8	8
Federal31- 1A	nd	na	-44.8	-247.5	na	na	na	na	na	3.2	0.1	146	9	8
Union Gorit II-1	15.7	na	-42.5	-230.7	-26.5	-153.3	-22.8	-121.4	-24.9	3.0	0.3	161	20	18
Cutler [Andy'	's Mesa and	Hamilton Cr	eek fieldsl											
AM-11	nd	na	-33.7	-135.0	-28.3	-116.7	-25.4	-111.7	-25.8	na	na	na	na	na
AM-38	nd	-25.9	-30.0	-125.6	-30.6	-124.3	-26.3*	-93.0*	-23.8*	2.6	0.2	195	18	20
AM-61	nd	-125.9	-32.6	-134.1	-24.3	-87.2	-20.4*	-33.0*	-20.5*	2.6	0.3	193	22	25
AM-62a	nd	na	_	_	-23.9	-78.9	-19.9	nd	nd	_			_	_
AM-62b	nd	-125.9	-32.7	-135.1	-24.3	-83.1	-21.7*	-29.0*	-23.9*	2.7	0.2	183	17	18
HC-1-36	nd	-60.3	-32.7 -32.3	-130.1	-24.3 -25.9	-63.1 -111.9	-21.7 -23.9	-29.0 -111.2	-23.9 -23.7	2.6	0.2	191	11	10
Honaker Trail					-23.9	-111.9	-23.9	-111.2	-23.7	2.0	0.1	191	11	10
AM-75a	nd	na		na	-28.5	-117.5	-24.7	nd	-24.5	na	na	no	na	na
AM-75b	nd	-33.0	na -34.3	–135.3	-28.5 $-28.7$	-117.3 -118.7	-24.7 -24.7	–111.3	-24.3 -24.1*	2.7	na 0.1	na 190	na 13	na 14
FF-4-20	na	na	-32.6	-130.2	-30.7	na	-25.0	na	na	na	na	na	na	na
FF-4-20	na	na 40.7	-32.5	-130.2	-30.5	na	-25.3	na	na	na	na	na	na	na
HC12-13	nd	-48.7	-34.4	-129.6	na	na	na or or	na	na -20.3*	5.2 2.7	0.3	47	13 19	13
HC-30-11 HC-25-22	−7.0 −7.4	na -52.6	-32.0 $-32.6$	$-128.2 \\ -128.2$	-33.0 $-32.3$	$-122.8 \\ -140.0$	-25.0* -23.9*	nd nd	-20.3* -20.4*	3.0	0.2 0.1	182 160	9	18 9
		-32.0				*	-23.9	iiu						
HC-36-23	-7.1	na	-34.2	-128.8	-29.1	-130.0 *	-24.6	nd	-23.1*	3.0	0.3	163	24	22
HC-36-34	-6.8	-41.0	-34.7	-128.5	-30.0	-135.0 *	-24.9	nd	-23.2*	3.0	0.3	163	20	18
Honaker Trail	l [Lisbon Va	lley field]												
MM31-42	nd	-47.0	-25.6	-108.2	-32.0	-138.3	-28.5	-106.8	-27.7	2.5	0.7	200	79	56
MM26-34	nd	-38.2	-43.0	-194.9	-31.7	-134.6	-28.7	-106.9	-27.7	1.7	0.3	297	50	41
MM36-14	na	na	-29.6	-27.9	na	na	na	na	na	na	na	na	na	na
BI24-31	nd	-48.1	-45.2	-231.9	nd	nd	nd	nd	nd	2.9	0.2	165	13	12
BH10-31	nd	-74.9	-42.6	-197.2	-30.2	-127.5	-27.2	-105.5	-26.5	na	na	na	na	na
Paradox [Great	ater Aneth f	ield]												
Sahgzie 1	nd	-32.9	-45.5	-284.1	-36.4	-199.7	-32.6	-143.1	-30.4	0.9	0.4	485	155	100
Monument- 8n-2	nd	-34.6	-44.9	-259.7	-36.2	-186.8	-32.7	-140.1	-30.7	0.3	0.5	825	na	323
Leadville/McG	Cracken [Lis	sbon Valley i	field]											
McIntyre 17- 21	-7.0	-80.6	-37.1	-130.1	-28.5	-118.0	-25.6	-111.7	-24.0	2.1	0.3	247	43	36
Lisbon B-610	-7.4	-67.3	-37.7	-155.7	-32.5	-130.9	-29.2	-108.1	-27.9	2.0	0.3	264	40	34
Lisbon D8-	-7. <del>4</del> -6.9	-59.6	-37.7 -41.4	-154.6	-34.1	-130.9 $-106.3$	-29.2 $-29.4$	-100.1 $-101.6$	-27.9 $-27.2$	2.0	0.3	261	34	30
10	0.5	03.0	11.1	10 1.0	0 1.1	100.0	27.1	101.0	27.2	2.0	0.2	201	01	50
Lisbon B8-10	-8.4	-63.2	-47.5	-216.7	-36.1	-135.3	-32.2	-114.3	-30.0	1.3	0.3	374	65	49
Lisbon 10- 33a	-7.8	-35.1	-45.7	-192.3	-35.0	-121.7	-31.1	-104.2	-28.9	na	na	na	na	na
Lisbon 10- 33b	-9.0	-29.2	-45.8	-191.8	-35.4	-124.1	-31.4	-110.1	-29.2	2.0	0.2	256	28	25

 $<sup>2\</sup>sigma^2$  of  $\Delta^{13}$ CH<sub>3</sub>D based on 95% CI.

(Wang et al., 2015). Samples were then analyzed relative to a reference gas (commercially sourced methane 'AL1') for 7 to 12 acquisition cycles (sample-standard pairs). The  $\delta^{13} C$  and  $\delta D$  values of the reference gas (AL1) are reported in V-PDB and V-SMOW scale, calibrated against community reference NGS-1 and NGS-3, and the value of  $\Delta^{13} CH_3 D$  is calibrated by equilibrating a set of reference gas at 250 °C (Wang et al., 2015).

The values of  $\delta^{13}\text{C}$  and  $\delta D$  of methane were derived from the

measurements of isotopologue abundances. The ratio of isotopologues and the ratio of isotopes are transposable such that  $^{12}\text{C}/^{13}\text{C}$  is equivalent to  $[^{13}\text{CH}_3\text{D}/^{12}\text{CH}_4]$ , and D/H is equivalent to  $1/4[^{12}\text{CH}_3\text{D}/^{12}\text{CH}_4]$ .

 $\Delta^{13}CH_3D$  represents the deviation of the abundance of clumped isotopologue  $^{13}CH_3D$  from the stochastic distribution, such that

$$\Delta^{13}CH_3D = \ln \frac{[^{13}CH_3D][^{12}CH_4]}{[^{13}CH_4][^{12}CH_3D]}$$
 (1)

 $T_{13D}$  – Apparent temperatures.

nd – non-detected due to low molecular compositions.

na – not-analyzed.

<sup>&</sup>lt;sup>a</sup> δD<sub>H2O</sub> data from the "AM-62b" sample in the same Andy's Mesa field with corresponding geological formation.

Carbon and/or hydrogen isotope data obtained online via GC-C-IRMS and/or GC-P-IRMS.

and is reported in per mil (%) units.

 $\Delta^{13}\text{CH}_3\text{D}$  at isotopic equilibrium as a function of temperature was computed via the following equation (valid above 270 K) from Eldridge et al. (2019):

$$\Delta^{13}CH_3D(T) \cong 1000 \times ln(K^{13}CH_3D) = \frac{1.47348 \times 10^{19}}{T^7} - \frac{2.08648 \times 10^{17}}{T^6} + \frac{1.19810 \times 10^{15}}{T^5} - \frac{3.54757 \times 10^{12}}{T^4} + \frac{5.54476 \times 10^9}{T^3} - \frac{3.49294 \times 10^6}{T^2} + \frac{8.89370 \times 10^2}{T}$$
(2)

These  $\Delta^{13}\mathrm{CH_3D}$ -based temperatures (T) are herein called 'apparent temperatures ( $T_{13D}$ ).

 $\delta D$  values of formation water ( $\delta D_{H2O};$  Table 2) from corresponding wells were previously reported in Kim et al. (2022a).  $\delta D_{H2O}$  values were measured at the University of Arizona via laser spectrometer (Los Gatos Research DLT-100 Liquid Water Isotope Analyzer) with a precision of 0.5‰ or isotope ratio mass spectrometer (Finnigan Delta S) with a precision of 1.0‰.

Forward models for  $\Delta^{13} \text{CH}_3 \text{D}$  were constructed based on the burial/thermal histories of the basin (Fig. 2) to calculate the temporal evolution of methane isotopologue compositions using equilibrium fractionation factors and the rate of hydrogen (D/H) isotope exchange between CH<sub>4</sub> and H<sub>2</sub>O. Model inputs are initial isotope and isotopologue compositions of methane ( $\delta^{13} \text{C}$ ,  $\delta \text{D}$ , and  $\Delta^{13} \text{CH}_3 \text{D}$ ) and the thermal histories of source rocks in different locations and depths of the basin. Hydrogen equilibrium fractionation factors for CH<sub>4</sub> in gas phase and H<sub>2</sub>O as a function of temperature (T in Kelvin) were calculated using the following equations valid from 3 to 200 °C from Turner et al. (2021):

$$1000 \times \ln^{D} a_{CH4(g)-H2O(l)} = -\frac{7.9443 \times 10^{12}}{T^{4}} + \frac{8.7772 \times 10^{10}}{T^{3}} - \frac{3.4973 \times 10^{8}}{T^{2}} + \frac{5.4398 \times 10^{5}}{T} - 382.05$$
(3)

Isotopic exchange rate followed abiotic exchange rate constants (units of  $\ln(\sec^{-1} [\text{mol/L}]^{-1})$  versus 1000/T (K<sup>-1</sup>)) from Turner et al. (2022):

$$ln(k_r) = -17.32 \times (1000/T) + 3.19 \tag{4}$$

The approach is similar to Beaudry et al. (2021) who calculated the equilibration timescales at constant temperatures. Here, we used the source rocks' thermal history from basin models, which were based on Rock-Eval pyrolysis and vitrinite reflectance (Nuccio and Condon, 1996) and apatite (U-Th)/He age data (Hoffman, 2009), and applied updated isotopic exchange rates and fractionation factors (Turner et al., 2021; Turner et al., 2022). The forward model was applied for three different parts of the basins: 1) Cane Creek source rocks of the Paradox Formation in the Lisbon Valley field, northeastern side of the basin (Nuccio and Condon, 1996); 2) Ismay-Desert Creek source rocks of the Paradox Formation in the Greater Aneth field, southwestern side of the basin (Nuccio and Condon, 1996); and 3) Cretaceous sediments in the Cisco field (based on thermochronology constraints from the Hay Canyon area, Book Cliffs; Hoffman, 2009).

#### 4. Results

#### 4.1. Traditional molecular and isotope ratios of natural gas

Measured molecular and isotopic composition of natural gas samples from six different reservoirs across the Paradox Basin are reported in Tables 1 and 2. Gas samples were collected from within the Ismay-Desert Creek source rocks of Paradox Formation in the southwestern part of the basin (e.g., Greater Aneth field), while gas samples were collected from

several reservoirs above/below the Cane Creek source rocks of the Paradox Formation in the northeastern part of the basin (Lisbon, Andy's Mesa, and Hamilton Creek fields) and Cisco field. Methane (CH<sub>4</sub>) is the dominant component in most gas samples (51.3–96.6 mol%), except for the Lisbon D8-10 sample with 29.0 mol% CH<sub>4</sub> and a remarkable 49 mol % CO<sub>2</sub> (Table 1). Gases have variable amounts of C<sub>2</sub> (0.01–16.2 mol%), C<sub>3</sub> (0.01–13.7 mol%), and  $_{n}$ C<sub>4</sub> (0.01–6.8 mol%) (Table 1). The methane to higher chain hydrocarbons ratios (CH<sub>4</sub>/ $\Sigma$ C<sub>2+</sub> or dryness) range from 1.4 to 61, except for the BI24-31 sample with 3204 (Table 1 and Fig. 3).

 $\delta^{13}C_{CH4}$  values for all samples range from -50.6 to -25.6% (Table 2 and Fig. 3). The  $\delta^{13}C_{C2}$  values for all samples range from -36.4 to -23.6% , while the  $\delta^{13}C_{C3}$  values range from -32.7 to -18.8% and are more positive than their respective  $\delta^{13}C_{C2}$  values (Table 2 and Fig. 4). The  $\delta^{13}C_{nC4}$  values range from -30.7 to -20.3%. The variation of  $\delta^{13}C$ values of CH<sub>4</sub> through C<sub>4</sub> for each gas sample was compared to expected trends for natural gas derived from a single source without post-genetic alteration and/or mixing effects (dashed straight lines in Fig. 4; Rooney et al., 1995; Chung et al., 1988; and Burruss and Laughrev, 2010). The gases from the shallower Dakota, Morrison, Cutler, and Honaker Trail formations have lower  $C_2$  and  $C_3$  concentrations and higher  $\delta^{13}C_{C_2}$  and  $\delta^{13}C_{C3}$  values than those from deeper Paradox, Leadville, and McCracken formations (Fig. 5A-5C). The isotopic difference between  $\delta^{13}C_{C2}$  and  $\delta^{13}C_{C3}$  (  $\Delta^{13}C_{C2/C3})$  of most samples is similar, while  $C_2/C_3$ molar ratios vary from 1 to 16 (Fig. 5D). δD<sub>CH4</sub> values for all samples range from -284.1 to -108.2% (Fig. 6A).

Relatively high CO<sub>2</sub> (0.5-4.3 mol%, Table 1) concentrations from the Dakota and Morrison formations exhibit very high  $\delta^{13}C_{CO2}$  values of 14.1 to 22.5‰ (Table 2 and Fig. 6B). Gases from the Leadville and McCracken formations contain the highest He (0.2-0.8 mol%), Ar (0.02-0.09 mol%), N2 (11-16 mol%), and CO2 (1.2-49 mol%, a median 3.7 mol%) concentrations in this study (Table 1) with  $\delta^{13}C_{CO2}$  values of -8.3 to -6.9% (Table 2 and Fig. 6B).  $CO_2$  concentrations from the Honaker Trail Formation in the Hamilton Creek field are higher (up to 0.7 mol%) than the same formation in Lisbon Valley and Andy's Mesa fields (<0.3 mol%). Their  $\delta^{13}C_{CO2}$  values (-7.4 to -6.8%) are nearly identical to those from the Leadville and McCracken formations. Gases from the Cutler Group also exhibit high He (0.1-0.4 mol%), Ar (0.03-0.19 mol%), and N<sub>2</sub> (7-19 mol%), but low CO<sub>2</sub> (0.01-0.09 mol%) concentrations (Table 1), CO<sub>2</sub> concentrations from some formation gases (Cutler Group and Honaker Trail Formation in the Lisbon Valley field and the Paradox Formation in the Greater Aneth field) were too low for  $\delta^{13}C_{CO2}$  analysis.

#### 4.2. Clumped isotopologues of methane

The abundance of  $\Delta^{13}\text{CH}_3\text{D}$  can help constrain the temperature at which methane was formed and/or last equilibrated (Ono et al., 2014; Wang et al., 2015; Xie et al., 2021). Methane clumped isotopologue ( $\Delta^{13}\text{CH}_3\text{D}$ ) values for the Dakota and Morrison formations range from 3.0 to 4.5‰, corresponding to apparent temperatures ( $T_{13D}$ ) between 76 and 162 °C (Table 2 and Fig. 7A). The  $\Delta^{13}\text{CH}_3\text{D}$  values for gases from the Cutler Group and/or Honaker Trail Formation are consistent (2.4 to 2.9‰), corresponding to  $T_{13D}$  from 161 to 202 °C, except for the HC12-13 ( $\Delta^{13}\text{CH}_3\text{D} = 5.2$ ‰;  $T_{13D} = 47$  °C) and MM26-34 ( $\Delta^{13}\text{CH}_3\text{D} = 1.7$ ‰;  $T_{13D} = 297$  °C) samples. Gases from the Paradox Formation have very low  $\Delta^{13}\text{CH}_3\text{D}$  values (0.9 and 0.3‰) corresponding to environmentally unrealistic  $T_{13D}$  (485 and 825 °C, respectively). Gases from the Leadville and/or McCracken formations also show low consistent  $\Delta^{13}\text{CH}_3\text{D}$  values (2.0–2.1‰), corresponding to  $T_{13D}$  from 247 to 264 °C, except for the Lisbon B8-10 sample with a lower  $\Delta^{13}\text{CH}_3\text{D}$  (1.3‰;  $T_{13D} = 374$  °C).

 $\Delta^{13} CH_3 D$  values were plotted versus the isotopic enrichment factor (\$\epsilon\$) between \$\delta D\$ values of methane and formation water (\$\epsilon\_{methane/water}\$) (Fig. 7B). The isotopic equilibrium curve, shown in Fig. 7B was calculated using the \$\Delta^{13} CH\_3 D\$ (Eq. (2) and \$\epsilon\_{methane/water}\$) (Eq. (3) calibrations given by Eldridge et al. (2019) and Turner et al. (2021), respectively. Gases from the Paradox Formation in the Greater Aneth field plot below

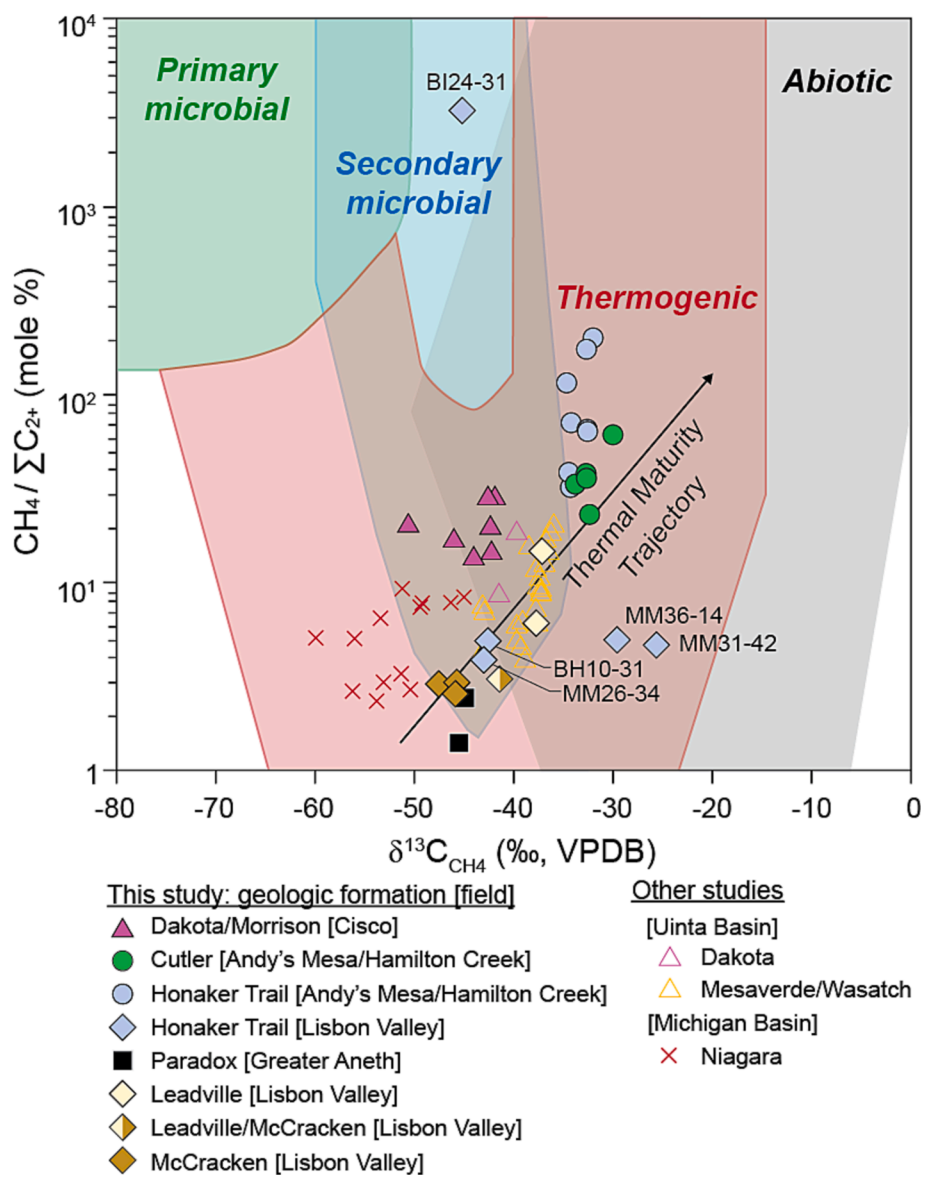


Fig. 3.  $\delta^{13}C_{CH4}$  versus CH<sub>4</sub>/ $\Sigma C_{2+}$  of the 'Bernard plot' with distinct sections of microbial, thermogenic, and abiotic gases as well as a thermal maturation trend (Bernard et al., 1976; Giunta et al., 2019; Milkov and Etiope, 2018; McIntosh et al., 2018). Thermogenic gas data from the Dakota and Mesaverde/Wasatch formations of the Uinta Basin (Zhang et al., 2009) and Silurian Niagara Formation of the Michigan Basin (Martini et al., 1998; Giunta et al., 2019).

the isotopic equilibrium curve, while gases from the Dakota and Morrison formations in the Cisco field and the Honaker Trail and McCracken formations in the Lisbon Valley field plot close to the equilibrium curve. Gases from the Cutler Group and Honaker Trail Formation in the Andy's Mesa and Hamilton Creek fields and Leadville Limestone in the Lisbon Valley field plot above the equilibrium curve. One of the Honaker Trail Formation samples (HC12-13) from the Hamilton Creek field plots far from the equilibrium curve with an anomalously high  $\Delta^{13}\text{CH}_3\text{D}$  (5.2%) value.

The evolution of  $\Delta^{13}\text{CH}_3\text{D}$  values through geologic time was modeled for three fields (Lisbon Valley, Greater Aneth, and Cisco fields) using their thermal histories of source rocks from basin models and a rate of abiotic hydrogen (D/H) isotope equilibration between methane and water (Turner et al., 2022) (Fig. 8). In the models for the Lisbon Valley field, methane in the Cane Creek source rocks of the Paradox Formation was equilibrated during maximum burial ( $\sim 30-80$  Ma) at 160 to 170 °C (Fig. 8A). Hydrogen isotopes of methane and water within the source rocks in the Lisbon Valley field were isotopically equilibrated for  $\sim 30$  m.y. during maximum burial ( $\sim 30-60$  Ma). In the models for

the Greater Aneth field, the  $\Delta^{13}CH_3D$  and  $\epsilon_{methane/water}$  values of methane, in the Ismay-Desert Creek source rocks of the Paradox Formation, slightly increased during burial (25-80 Ma; up to 110 °C), but never reached equilibrium, and then maintained their values after cooling (Fig. 8B). In the models for the Cisco field, three thermal histories for the Cretaceous sediments were applied to the models, starting around 100 Ma, during maximum burial with different initial maximum temperatures ( $T_0 = 110$ , 140, or 160 °C) (Fig. 8C). While the model starting at 110 °C T<sub>0</sub> never achieved Δ<sup>13</sup>CH<sub>3</sub>D equilibrium, the models starting at 140 and 160 °C reached  $\Delta^{13}$ CH<sub>3</sub>D equilibrium during maximum burial until 50–60 Ma. The model results starting at 160  $^{\circ}$ C T $_{0}$ show hydrogen isotopic equilibrium between methane and water during the (first) maximum burial ( $\sim$ 60–70 Ma), while those starting at 140  $^{\circ}$ C T<sub>0</sub> exhibit hydrogen isotopic equilibrium during the secondary burial maximum ( $\sim$ 10–50 Ma). The three modeled  $\Delta$ <sup>13</sup>CH<sub>3</sub>D results at present (3.1–3.4‰) are within the range of the measured  $\Delta^{13}CH_3D$  values (2.9-4.4%).

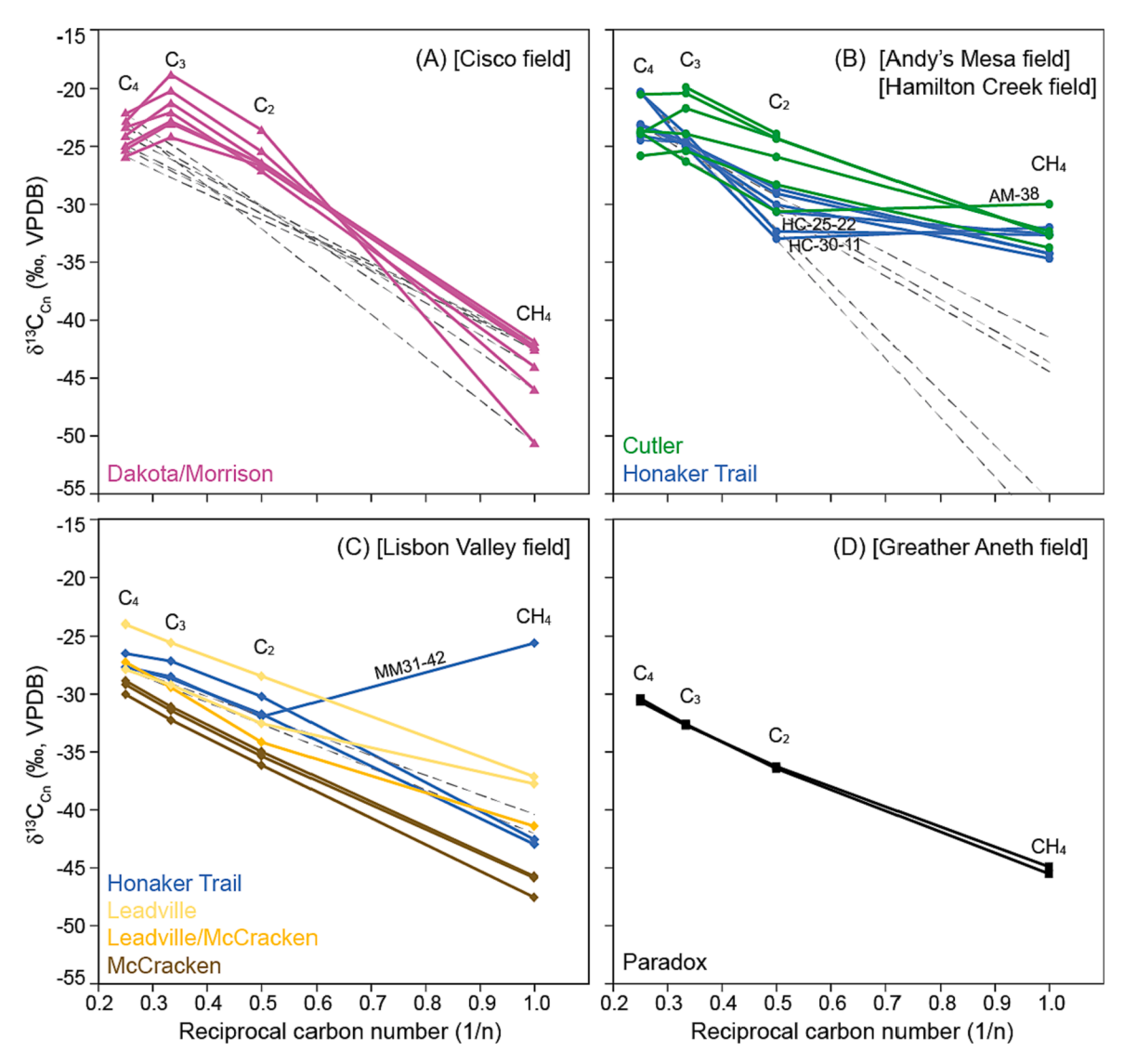


Fig. 4.  $\delta^{13}C_{Cn}$  (n = 1 to 4) as a function of the reciprocal carbon number (1/n) of hydrocarbons of each sample. A-D diagrams display specific fields with various reservoirs shown in different colored lines. The dashed straight line for select gas samples represents the expected  $\delta^{13}C$  trend for natural gases derived from a single source without post-genetic alteration and/or mixing effects (e.g., Chung et al., 1988; Rooney et al., 1995; Burruss and Laughrey, 2010).

# 5. Discussion

#### 5.1. Thermogenic origin of most natural gas

Natural gases in oil and gas reservoirs across the Paradox Basin plot within the thermogenic gas field in the 'Bernard plot' (Fig. 3; Bernard et al., 1976; Milkov and Etiope, 2018) with low  $\text{CH}_4/\Sigma C_{2+}$  and high  $\delta^{13}C_{\text{CH4}}$  values, indicating natural gases are predominantly thermogenic in origin. Many of the thermogenic gases appear to have originated from a single source rock, as their  $\delta^{13}C_{\text{Cn}}$  values follow a straight trend in Fig. 4 (e.g., Honaker Trail and Leadville/McCracken formations in the Lisbon Valley field and Paradox Formation in the Greater Aneth field). Both  $\Delta^{13}C_{\text{C2/C3}}$  and  $C_2/C_3$  molar ratios of most natural gases are within the range of modeled values for the secondary cracking of oil from Type II kerogen at 200 °C (Prinzhofer and Huc, 1995; Lorant et al., 1998) (Fig. 5D). Many of the  $\Delta^{13}C_{\text{H3}}$ D (and apparent methane formation temperatures,  $T_{13D}$ ) and  $\delta^{13}C_{\text{CH4}}$  values are also within the prior range of thermogenic gases from other basins (Wang et al., 2015; Douglas et al., 2016, 2017; Giunta et al., 2019; McIntosh et al., 2018) (Fig. 7A).

The predominance of thermogenic gas is consistent with the deep burial history of black shale source rocks, interbedded in evaporite

confining units in the Paradox Formation, throughout most of the basin. The sterilization of shale source rocks and adjacent conventional reservoirs during maximum burial (>80 °C; Head et al., 2003; Wilhelms et al. 2001) and lack of meteoric water influx (Kim et al., 2022a, 2002b) likely precluded widespread microbial gas generation in the organic-rich shales (McIntosh et al., 2023).

# 5.2. Different thermal maturities of hydrocarbons

Most natural gases in the Paradox Basin follow a typical thermal maturation trend in gas molecular and isotopic composition (Giunta et al., 2019; Milkov and Etiope, 2018; McIntosh et al., 2018) with increasing thermal maturity (Figs. 3 and 5C). The thermogenic gas trend in the  $\delta^{13}C_{C2}$  versus  $\delta^{13}C_{C3}$  plot (Fig. 5C) (Martini et al., 2003; Osborn and McIntosh, 2010) shows similar differences in thermal maturity from the CH<sub>4</sub>/ΣC<sub>2+</sub> versus  $\delta^{13}C_{CH4}$  plot (Fig. 3). For example, oil-associated gases from the Paradox Formation in the Greater Aneth field, in the southwestern part of the basin, show the lowest thermal maturity with relatively wet gas (1.4 and 2.4 of CH<sub>4</sub>/ΣC<sub>2+</sub>) and low  $\delta^{13}C_{CH4}$  (–45.2  $\pm$  0.4‰),  $\delta^{13}C_{C2}$  (–36.3  $\pm$  0.1‰), and  $\delta^{13}C_{C3}$  (–32.7  $\pm$  0.1‰) values, compared to other samples in the basin. The anomalously low  $\Delta^{13}CH_3D$ 

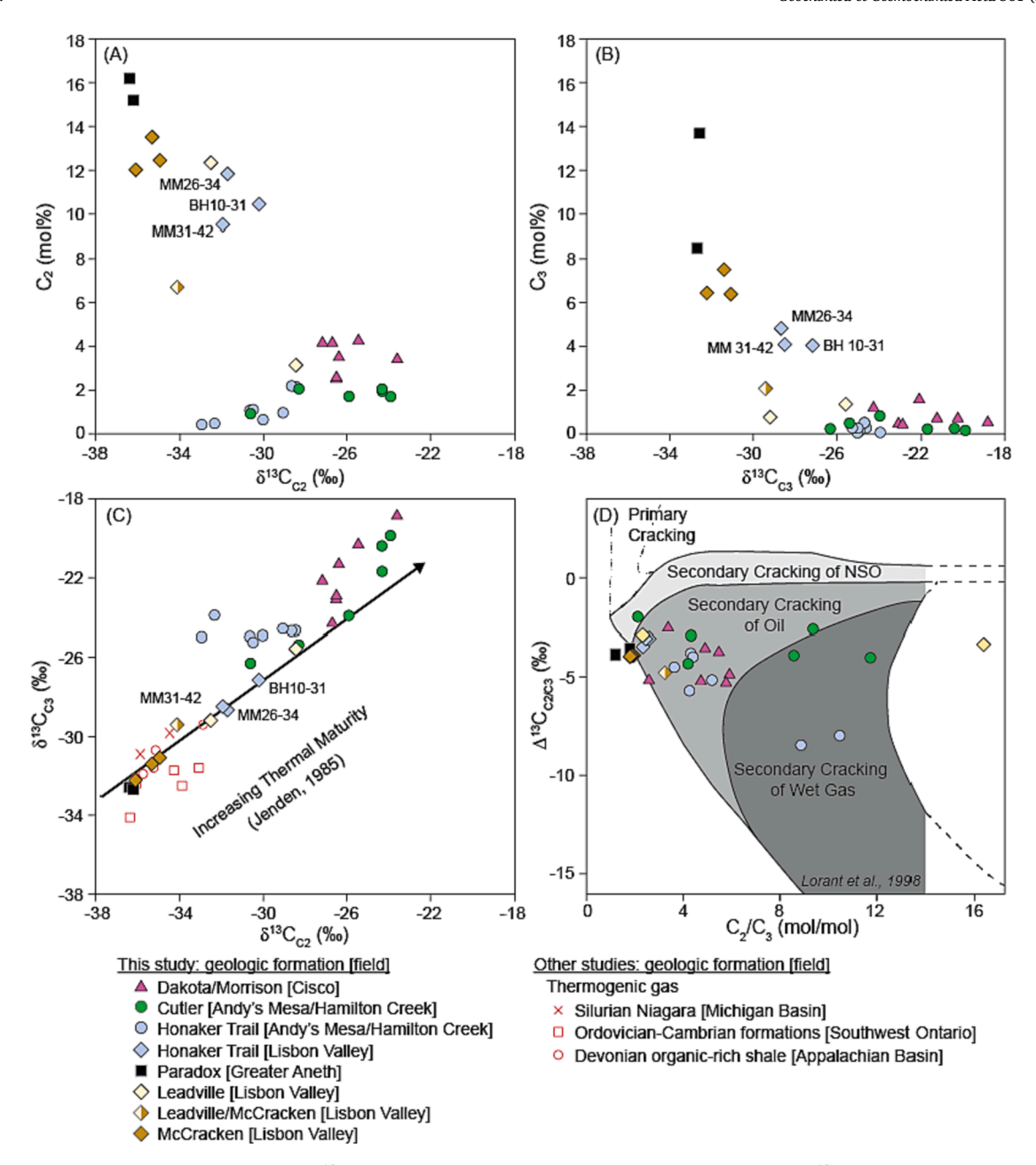


Fig. 5. (A) Ethane ( $C_2$ ) concentration (mole %) versus  $\delta^{13}C$  values of  $C_2$ . (B) Propane ( $C_3$ ) concentration (mole %) versus  $\delta^{13}C$  values of  $C_3$ . (C) C isotopic relationship between  $C_2$  and  $C_3$ . Thermogenic gas data from Ordovician-Cambrian formations in southwestern Ontario and Silurian Niagara Formation in the Michigan Basin (Giunta et al., 2019), and Devonian organic-rich shales in the Appalachian Basin (Osborn and McIntosh, 2010). (D) Evolution of the maturity model at 200 °C with four thermal maturity zones (Lorant et al., 1998).

values (Fig. 7), corresponding to unrealistically high  $T_{13D}$  (485 to 825 °C) relative to the thermal history for the Paradox Formation in the Greater Aneth field (Fig. 2B), indicate that the relatively low-maturity thermogenic methane (Figs. 1B, 3, and 5C) never reached thermal equilibrium. This is reasonable considering the relatively shallow burial depths of source rocks (Ismay-Desert Creek member of Paradox Formation) with lower  $R_0 \leq 0.87\%$  (Fig. 1B) along the southwestern margin of the basin, compared to the deeply buried source rocks in the northeastern part of the basin (Fig. 2A). The high  $T_{13D}$  values are beyond the thermogenic gas window (300 °C), suggesting that disequilibrated  $\Delta^{13}$ CH<sub>3</sub>D cannot serve as a thermometer for methane generation, but rather as a proxy of thermal maturity (Xie et al., 2021). In addition, this study extends the minimum range of  $\Delta^{13}$ CH<sub>3</sub>D values for thermogenic gas beyond previous studies (Giunta et al., 2019; Douglas et al., 2017).

Relatively low to moderate thermal maturity gases were observed in

the Leadville and McCracken formations below source rocks (Cane Creek member of Paradox Formation) in the Lisbon Valley field (northeastern part of the basin), based on the increasing  $CH_4/\Sigma C_{2+}$  and  $\delta^{13}C_{CH4}$  values with decreasing stratigraphic depth. For instance, the McCracken Sandstone is the deepest (2.5–2.9 and  $-45.1\pm2.3\%$ ), followed by the Leadville/McCracken formations (3.1 and -41.4%) and the overlying Leadville Limestone (6.1–14.6 and  $-37.4\pm0.3\%$ ). The low to moderate thermal maturity gases may have come from early stages of hydrocarbon generation in the source rocks (Fig. 2A). This likely occurred during the deposition of evaporites and siliciclastic sediments and rapid burial, and the expulsion of hydrocarbons into underlying formations, in the deepest part of the sedimentary basin (Fig. 9B). The lack of higher maturity hydrocarbons in these deep reservoirs, suggests they may have been isolated from the overlying shale source rocks of the Paradox Formation, during the growth of the

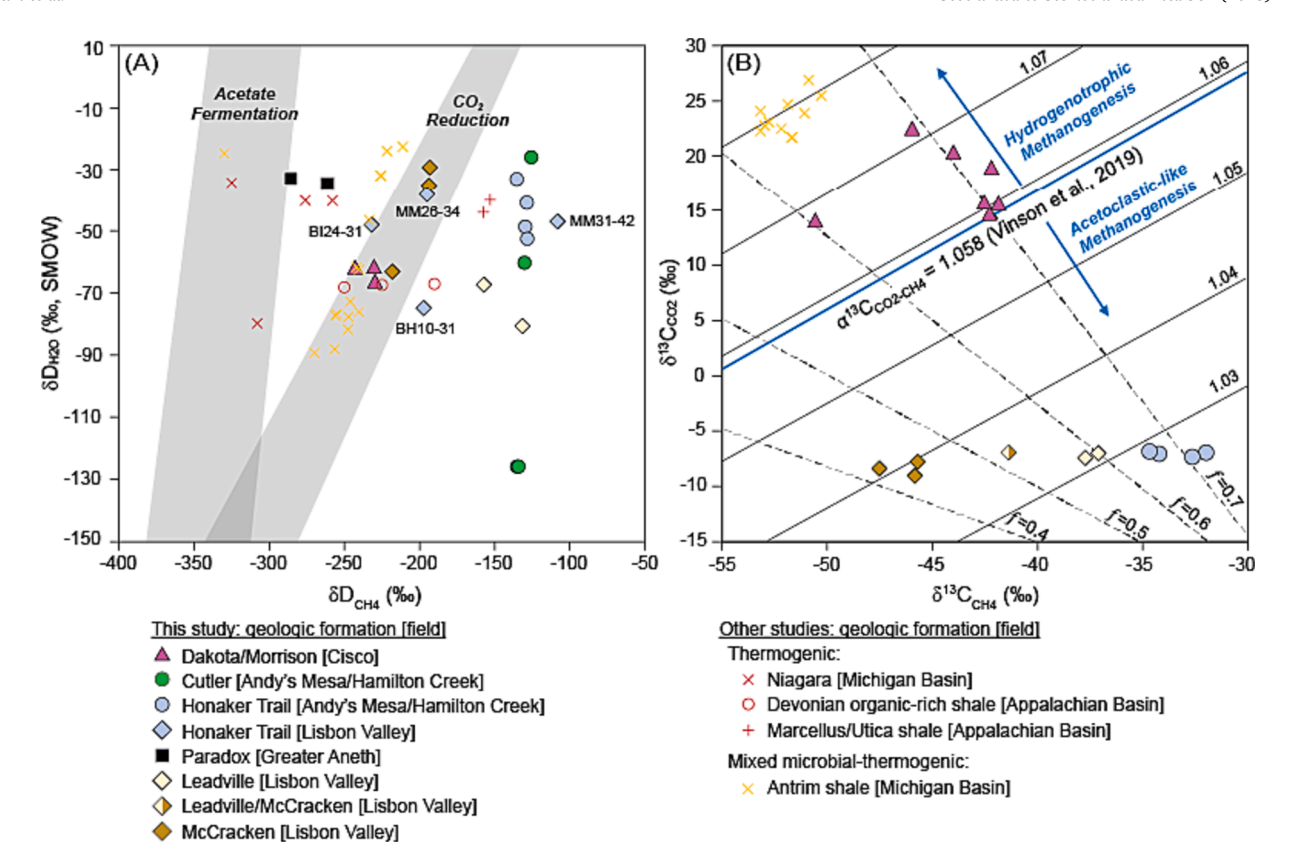


Fig. 6. (A)  $\delta D_{CH4}$  versus  $\delta D_{water}$  plot with hydrogen isotope fractionation trends of acetate fermentation and  $CO_2$  reduction (modified from Osborn and McIntosh, 2010) forming microbial gases. (B)  $\delta^{13}C_{CH4}$  versus  $\delta^{13}C_{CO2}$  plot with carbon isotope fractionation trends of hydrogenotrophic (i.e.,  $CO_2$  reduction) and acetoclastic-like (i.e., acetate fermentation) methanogenesis, distinguished by an alpha fractionation factor ( $\alpha^{13}C_{CO2-CH4}$ ) of 1.058 given by Vinson et al. (2019). Examples of thermogenic gases shown as red symbols are from the Silurian Niagara Formation in the Michigan Basin (Giunta et al., 2019), Devonian organic-rich shales in the Appalachian Basin (Osborn and McIntosh, 2010), and Marcelus/Utica shales in the Appalachian Basin (Wang et al., 2015). Examples of mixed microbial-thermogenic gases in yellow symbols are from the Devonian Antrim Shale in the Michigan Basin (Giunta et al., 2019; Stolper et al., 2015). Examples of microbial gases, shown as green symbols, are from the Santa Monica/Santa Barbara basins (Stolper et al., 2015), Northern Cascadia Margin, and Powder River Basin (Wang et al., 2015).

Paradox Formation salt walls. The calculated  $T_{I3D}$  values (247 to 374 °C; Fig. 7A) are also much higher than expected given the thermal/burial histories of the overlying source rocks ( $\sim$ <200 °C in Fig. 2A; Nuccio and Condon, 1996). The early generation, migration, and isolation of these natural gases from the source rocks may have prevented equilibration with  $\Delta^{13}$ CH<sub>3</sub>D. The methane isotopologues are likely recording apparent temperatures that reflect early thermogenic kinetic effects, not equilibrium conditions.

Thermogenic gases from the Honaker Trail Formation above the source rocks in the Lisbon Valley field are slightly more mature (low to moderate extents of thermal maturity) than gases in the Leadville and McCracken formations (Fig. 3).  $\delta^{13}C_{CH4}$  values of the Honaker Trail Formation in the Lisbon Valley field plot along the thermal maturity trend (BH10-33; MM26-34) or below the trend, except for the BI24-31 sample. The  $\Delta^{13}CH_3D$  values (2.5 and 2.9‰) correspond to 165 and 200 °C  $T_{13D}$ , respectively, except for the MM26-34 sample. These  $T_{13D}$  are within the thermogenic gas window (300 °C), indicating the thermally matured gases are equilibrated with  $\Delta^{13}CH_3D$  (Fig. 7A).

The Honaker Trail Formation samples (MM31-42; MM36-14) that plot below the thermal maturity trend were likely affected by very wet gas at a low level of maturity when the source rocks behaved as an open system (Burruss and Laughrey, 2010), based on low  $CH_4/\Sigma C_{2+}$  and high  $\delta^{13}C_{CH4}$  compared to  $\delta^{13}C_{C2+}$  values (Figs. 3 and 4C). In Fig. 5C, the MM31-42 sample falls on the thermogenic gas trend together with other Honaker Trail samples (MM26-34; BH10-31) with similar  $\delta^{13}C_{C2}$  and  $\delta^{13}C_{C3}$  values, supporting a similar degree of thermal maturity for gases from the same formation and field.

The BI24-31 sample with very high  $CH_4/\Sigma C_{2+}$  (Fig. 3) may have been

affected by solubility fractionation through interaction with fluids or migration fractionation during gas leakage or diffusion from source rocks leading to the loss of C<sub>2+</sub> hydrocarbons (Prinzhofer and Pernaton, 1997; Prinzhofer and Battani, 2003). The relatively high  $\Delta^{13}$ CH<sub>3</sub>D value of the BI24-31 sample, compared to other Honaker Trail samples in the Lisbon Valley field, also suggests the effects of diffusion (e.g., trajectory in Fig. 7A) (Douglas et al., 2017; Young et al., 2017). Alternatively, anaerobic oxidation of C2+ and/or biodegradation of crude oil, producing secondary microbial methane, in this oil-associated gas reservoir could explain the extremely low  $C_{2+}$  (0.01 mol%) and high  $CH_4$  (93 mol %) concentrations of the BI24-31 sample (Martini et al., 2003, 2008). It is notable that the  $\Delta^{13}\text{CH}_3\text{D},~\delta^{13}\text{C}_{\text{CH4}}\text{, and}~\epsilon_{methane/water}$  values of the BI24-31 sample are similar to the Dakota and Morrison formation reservoirs, which are interpreted to contain mixed thermogenic-microbial gases (See Section 5.3 below). The presence of relatively high  $\delta^{13}C_{C2+}$ and  $\delta^{13}C_{CO2}$  values could suggest anaerobic oxidation of hydrocarbons, coupled to secondary microbial methanogenesis (Martini et al., 2003; 2008), however the concentrations of C<sub>2</sub> and CO<sub>2</sub> of the BI24-31 sample were too low for  $\delta^{13}$ C analysis.

The thermally mature gases in the Honaker Trail Formation in the Lisbon Valley field, in the proximity of isotopic equilibrium in  $\Delta^{13} CH_3 D$  versus  $\epsilon_{methane/water}$  space (Fig. 7B), suggests that post-genetic alteration, resulting in equilibrium with hydrogen isotope exchange, occurred between methane and water or other hydrogen sources (e.g.,  $H_2 S$ ). The  $\Delta^{13} CH_3 D$  values of these thermogenic gases are similar to thermogenic gases in the deep, Silurian Niagara play in the Michigan Basin (Giunta et al., 2019), while the  $\epsilon_{methane/water}$  values are different. This implies that the thermal maturity of the gases in the Niagara

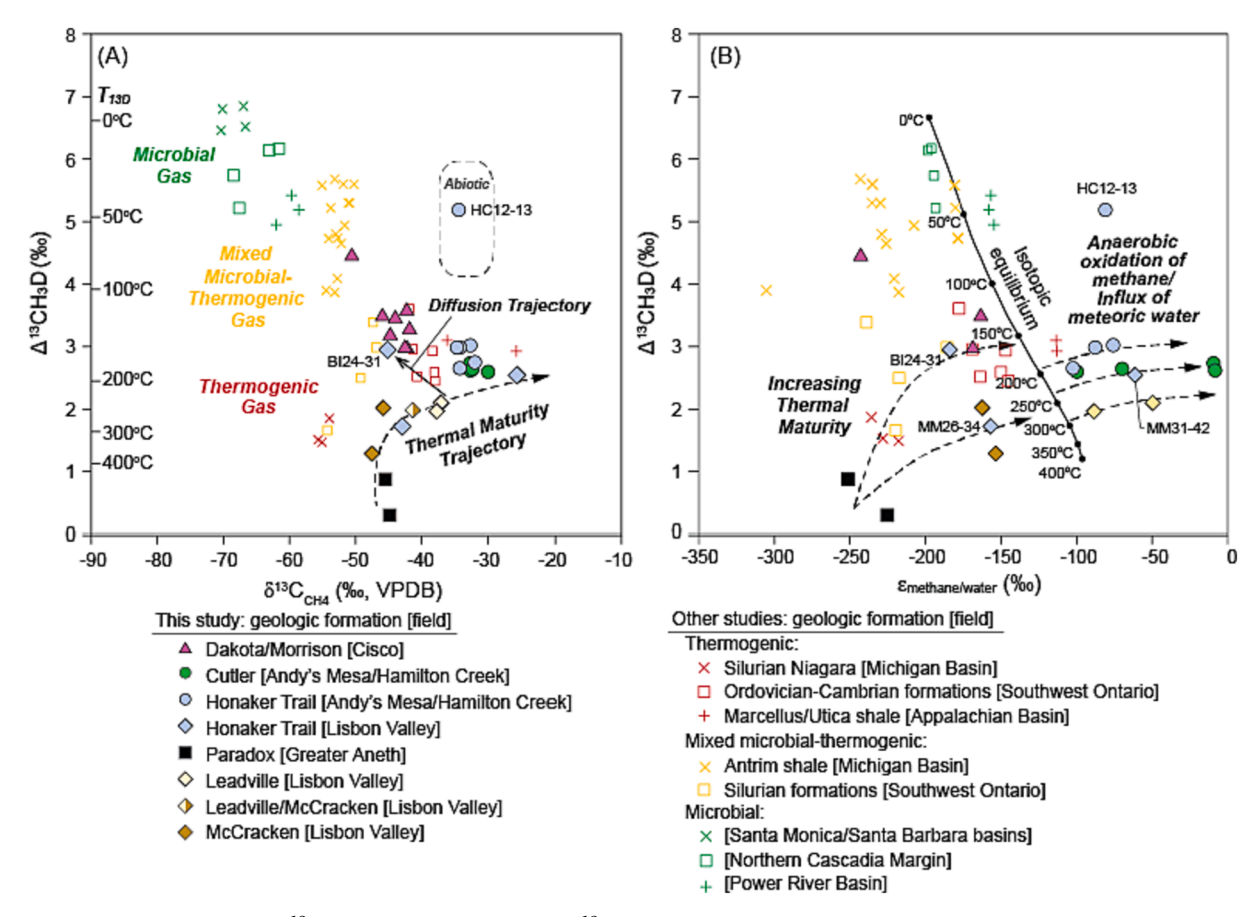


Fig. 7. (A) Methane clumped isotope ( $\Delta^{13}\text{CH}_3D$ ) values as a function of  $\delta^{13}\text{C}$  of methane with compiled fields for microbial, mixed microbial-thermogenic, and thermogenic gases in sedimentary basins (Stolper et al., 2014a, b; Stolper et al., 2015; Wang et al., 2015; Douglas et al., 2016; Young et al., 2017; Giunta et al., 2019; Shuai et al., 2018; McIntosh et al., 2018). Diffusion trajectory given by Douglas et al. (2017). (B) A plot of isotopic enrichment factor ( $\epsilon$ ) between  $\delta D_{\text{CH4}}$  and  $\delta D_{\text{H2O}}$  ( $\epsilon_{\text{methane/water}}$ ) versus  $\Delta^{13}\text{CH}_3D$  with equilibrium curve using the Turner et al. (2021 and 2022) calibrations (Eq. (2) and Eq. (3). Examples of thermogenic gases shown as red symbols from the Silurian Niagara Formation in the Michigan Basin, Ordovician-Cambrian formations in the southwestern Ontario (Giunta et al., 2019), and Marcelus/Utica shales in the Appalachian Basin (Wang et al., 2015). Examples of mixed microbial-thermogenic gases in the yellow symbols are from the Devonian Antrim Shale in the Michigan Basin and Silurian formations in the southwestern Ontario (Giunta et al., 2019; Stolper et al., 2015). Examples of microbial gases, shown as green symbols, are from the Santa Monica/Santa Barbara basins (Stolper et al., 2015), Northern Cascadia Margin, and Powder River Basin (Wang et al., 2015).

reservoir were slightly lower than that of gases in the deep reservoirs in the Lisbon Valley. Further studies of  $\Delta^{13} \text{CH}_3 \text{D}$  equilibrium and hydrogen isotopic exchange between methane and water, relative to the thermal and burial history of the Michigan Basin, and other sedimentary basins, are needed to evaluate the influence of thermal maturity versus postgenetic processes.

Very dry gas samples from the Cutler Group and Honaker Trail Formation in the Andy's Mesa and Hamilton Creek fields, in the northeastern part of the basin, have relatively high thermal maturity with increasing  $CH_4/\Sigma C_{2+}$  from 23 to 200 and consistently high  $\delta^{13}C_{CH4}$  $(-33.0 \pm 1.3\%), \ \delta^{13}C_{C2} \ (-28.6 \pm 2.9\%), \ \delta^{13}C_{C3} \ (-23.6 \pm 2.0\%)$ (Figs. 3 and 4C),  $\Delta^{13}\text{CH}_3\text{D}$  (2.6–3.0‰), and  $\epsilon_{methane/water}$  (–102.3 to -8.2%) (Fig. 6) values, compared to gases from the Honaker Trail Formation in the Lisbon Valley field. The high thermal maturity of gases suggests that, during maximum burial, hydrocarbons were generated from the source rock ( $R_0 \ge 3.05\%$ ) at relatively high temperatures (Fig. 2B) and migrated into the overlying formations (Fig. 9B). However, a gradual increase in dryness (from 4 to 200  $CH_4/\Sigma C_{2+}$ ), consistent  $\delta^{13}C_{CH4}$  values (~-33‰), and high  $\Delta^{13}CH_3D$  and  $\epsilon_{methane/water}$  values relative to the isotopic equilibrium curve (Fig. 7) evoke questions concerning the loss of hydrocarbons by physical processes, such as leaking or diffusion, the mixing of a dry gas with a wet gas from different sources, or post-genetic alteration of hydrocarbons by microbial activity.

Gases from the Dakota and Morrison formations (the shallowest

reservoirs in this study) in the Cisco field plot above the thermal maturity trend with relatively dry gas (14-29 of  $\text{CH}_4/\Sigma C_{2+}$ ) and low  $\delta^{13}C_{CH4}$  values of  $-44.3 \pm 2.7\%$  (Fig. 3) from mixing of moderately mature thermogenic gases with secondary microbial methane, as seen in previous studies (Zhang et al., 2009) (Fig. 3). The high  $\delta^{13}C_{C2}$  and  $\delta^{13}C_{C3}$ values ( $-26.0 \pm 1.1\%$  and  $-21.8 \pm 1.7\%$ , respectively) in Fig. 4C indicate high thermal maturity and/or post-genetic alteration (e.g., anaerobic oxidation of hydrocarbons), as discussed below. The thermogenic gases in the Cisco field were likely sourced from the Paradox Formation shale source rocks during maximum burial (80-100 Ma; Nuccio and Condon, 1996), and later migrated into overlying reservoirs during post-Cretaceous uplift of the upthrown block along the Uncompahgre Fault (Young, 1983) approximately 50-70 Ma (Fig. 2C). Alternatively, hydrocarbons may have been sourced from thermal maturation of carbonaceous shales in the Dakota and Morrison formations (Hendel, 1961) during maximum burial (Fig. 2C; Hoffman, 2009).

The  $\Delta^{13}\text{CH}_3\text{D}$  and  $\epsilon_{methane/water}$  values for gases from the Dakota and Morrison formations in the Cisco field (Fig. 7) are close to or overlap with mixed microbial-thermogenic gases from the Devonian Antrim Shale of the Michigan Basin and Silurian formations of the southwestern Ontario (Giunta et al., 2019; Stolper et al., 2015) and thermogenic gas from Ordovician-Cambrian formations in southwestern Ontario (Giunta et al., 2019). The overlapping values supports the low  $\Delta^{13}\text{CH}_3\text{D}$  range for mixed microbial-thermogenic gas.

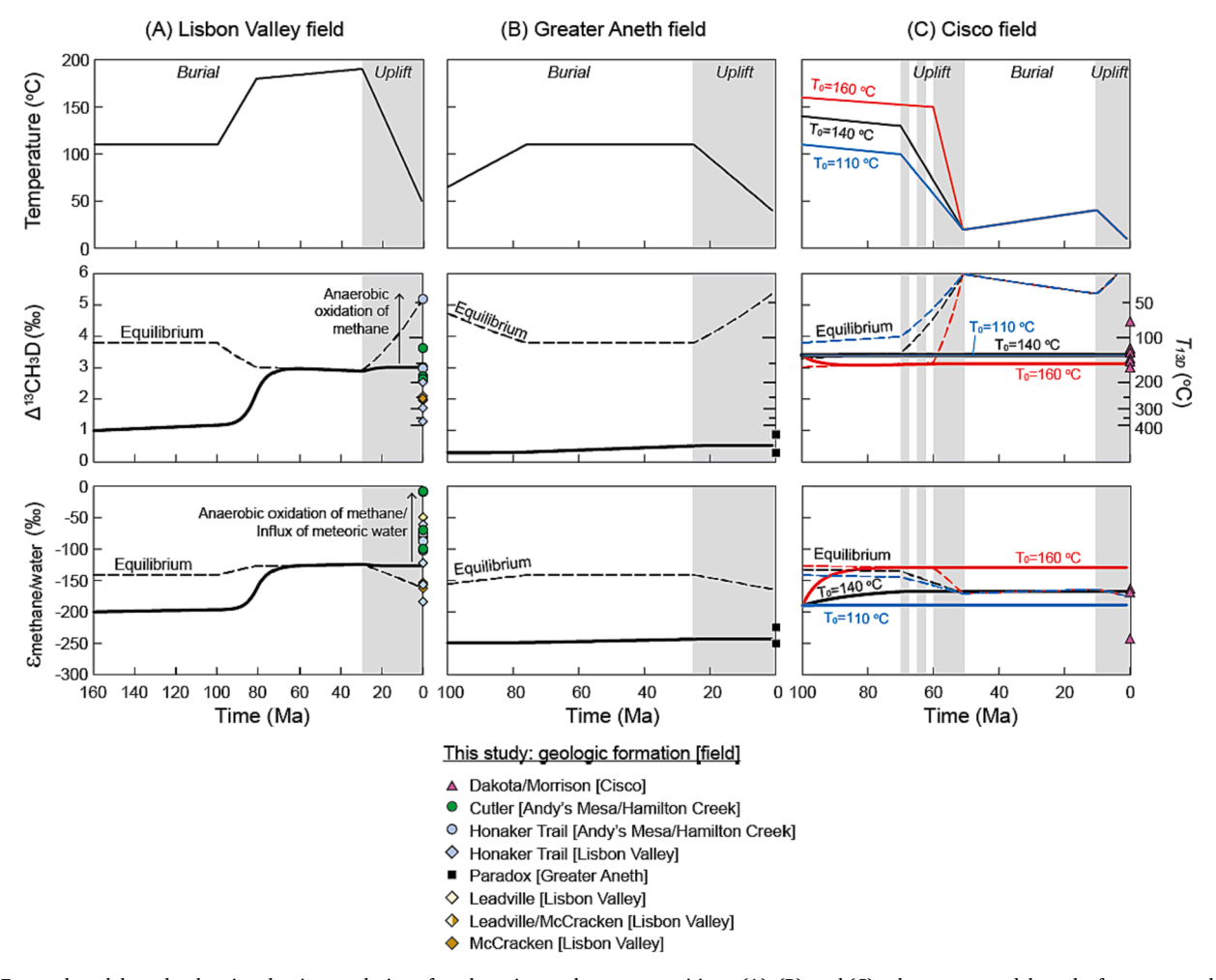


Fig. 8. Forward model results showing the time evolution of methane isotopologue compositions. (A), (B), and (C) columns are model results for source rocks in the Lisbon Valley field (northeastern side of the basin), Greater Aneth field (southwestern side of the basin), and Cisco field, respectively. The diagram at top shows the thermal history according to previous basin models. The diagram in the middle shows the time evolution of  $\Delta^{13}$ CH<sub>3</sub>D values and that expected from equilibrium (dashed line). The bottom diagram show  $\varepsilon_{\text{methane/water}}$  values and that expected from equilibrium (dashed line) depending on different initial temperatures (110°C in blue, 140°C in black, and 160°C in red) at 100 Ma. The measured  $\Delta^{13}$ CH<sub>3</sub>D and  $\varepsilon_{\text{methane/water}}$  values in this study are plotted at 0 Ma for comparison.

### 5.3. Biodegradation of hydrocarbons

Methane-dominated dry, thermogenic gases in the Dakota/Morrison (Cisco field) and Cutler and Honaker Trail formations (Andy's Mesa/Hamilton Creek fields) (Fig. 3) have high  $\delta^{13}C_{Cn}$  values, relative to the expected single source trend (Fig. 4A-4B), and plot above the thermogenic gas trends in both the 'Bernard plot' (Fig. 3) and the  $\delta^{13}C_{C2}$  versus  $\delta^{13}C_{C3}$  plot (Fig. 5C). Together, these isotopic shifts suggest the thermogenic gases have been altered by post-genetic biodegradation (e.g., Jenden and Kaplan, 1989; Rooney et al., 1995; Lorant et al., 1998).

Thermogenic gases in the Dakota/Morrison formations show a carbon isotopic reversal between  $C_3$  and  $_nC_4$  (Fig. 4A) with lower  $\delta^{13}C_{CH4}$  values compared to gases in other shallow reservoirs (e.g., Cutler Group and Honaker Trail Formation in Fig. 4B). Gases from the Cutler Group and Honaker Trail Formation in the Andy's Mesa and Hamilton Creek fields also have relatively high  $\delta^{13}C$  values for CH $_4$  compared to what is expected for a single source trend (Fig. 4B).  $\delta^{13}C_{C3}$  values for half of these gases are nearly identical to  $\delta^{13}C_{C4}$  values. The HC-25-22 and HC-30-11 samples show a carbon isotopic reversal between CH $_4$  and  $C_2$  with relatively high  $\delta^{13}C_{CH4}$  and low  $\delta^{13}C_{C2}$  values. The AM-38 sample shows a carbon isotopic reversal between CH $_4$  and  $C_2$  due to an elevated  $\delta^{13}C_{CH4}$  value. The MM31-42 sample from the Honaker Trail Formation in the Lisbon Valley field shows a carbon isotopic reversal between CH $_4$  and  $C_2$  (Fig. 4C). The anaerobic oxidation of  $C_{2+}$ , particularly  $C_3$ , by

microbial activity with selective consumption over other alkanes (James and Burns, 1984; Wenger et al., 2002; Martini et al., 1998, 2003, and 2008) can explain low molecular and high isotopic compositions of C<sub>2</sub> and C<sub>3</sub> (Fig. 5A and 5B) in these shallow gas reservoirs.

Anaerobic oxidation of methane (AOM) could have led to increasing disequilibrium in  $\Delta^{13}$ CH<sub>3</sub>D and  $\varepsilon_{\text{methane/water}}$  values for gases from the Cutler Group and Honaker Trail Formation in the Andy's Mesa and Hamilton Creek fields (Fig. 7B; Giunta et al., 2022). However, the disequilibrium in  $\epsilon_{methane/water}$  values may be mainly due to different water sources in each reservoir. For example, the Cutler Group samples with the lowest  $\delta D_{H2O}$  values (-125.9%), representing meteoric waters (Fig. 6A), exhibit the highest  $\varepsilon_{\text{methane/water}}$  values (-8.2 and -9.2%) with significant disequilibrium (Fig. 7B). In contrast, reservoirs containing older, saline fluids (e.g., Leadville and McCracken formations in Lisbon Valley), with higher  $\delta D_{\text{H2O}}$  values, have lower  $\epsilon_{\text{methane/water}}$ values. The deviations from the equilibrium curve in  $\Delta^{13}\text{CH}_3\text{D}$  and  $\epsilon_{methane/water}$  space (Fig. 7B) can serve as a new model for identification of thermogenic gases formed in the wet-gas window (plotting far below the equilibrium curve) versus biodegradation of dry-gases without generation of secondary microbial methane (plotting above the curve).

# 5.4. Microbial methanogenesis

The Dakota and Morrison reservoirs in the Cisco field have relatively

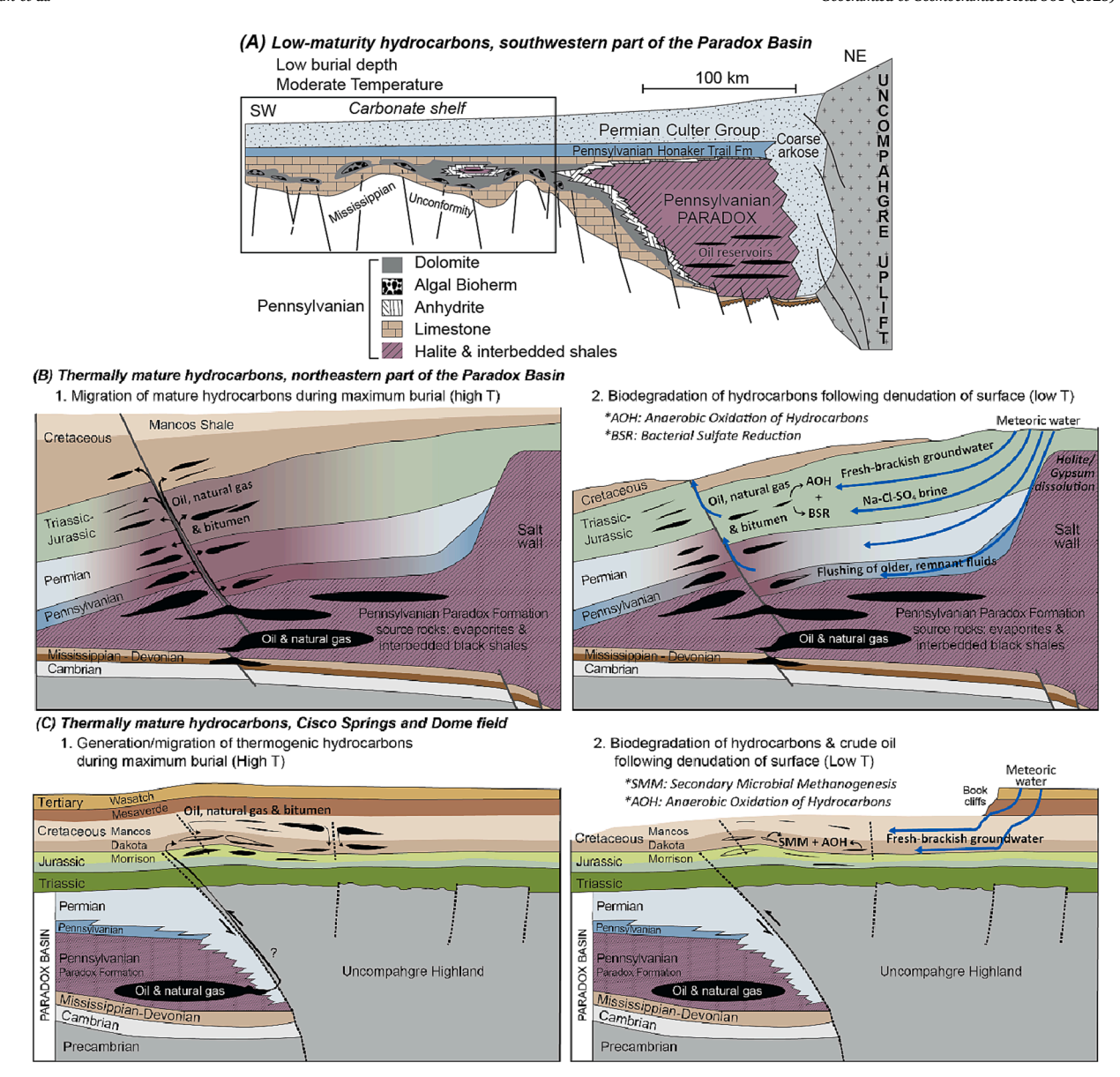


Fig. 9. (A) Schematic cross-section A-A' in Fig. 1A during the Permian, modified from Whidden et al. (2014) and Stevenson and Baars (1985). Low-maturity hydrocarbons in the black shale source rocks of the Paradox Formation at relatively shallow depth in the southwestern part of the Paradox Basin. (B) 1. Migration/Expulsion of thermally mature hydrocarbons from black shale source rocks of the Paradox Formation into overlying/underlying formations through faults at maximum burial and high temperature. 2. Following recent denudation of the Colorado Plateau (<4–10 Ma), lower temperatures and deep meteoric circulation (Kim et al., 2022b) promoted anaerobic oxidation of hydrocarbons (AOH), likely coupled to bacterial sulfate reduction (BSR) in shallow reservoirs. (C) Schematic cross-section in Cisco Springs and Dome field modified from Young (1983). 1. Generation and migration of thermogenic hydrocarbons in the Cretaceous and Jurassic sediments in the Cisco field. 2. Biodegradation of hydrocarbons and crude oil, producing secondary microbial methane (SMM) by active meteoric circulation and low temperature following uplift and the recent denudation.

low  $\delta^{13}C_{CH4}$  values ( $-44.3\pm2.9\%$ ; Figs. 3 and 4A) and high CO<sub>2</sub> concentrations ( $2.1\pm1.4$  mol%; Table 1) enriched in  $^{13}C$  ( $17.4\pm3.0\%$   $\delta^{13}C_{CO2}$ ; Table 2), consistent with microbial methanogenesis. The  $\delta D$  values of CH<sub>4</sub> and co-produced H<sub>2</sub>O (Fig. 6A) and  $\delta^{13}C$  values of CH<sub>4</sub> and CO<sub>2</sub> (Fig. 6B) from the Dakota and Morrison formations suggest microbial methane was generated via CO<sub>2</sub> reduction (i.e., hydrogenotrophic methanogenesis). Deeper gases from the McCracken and Honaker Trail formations in the Lisbon Valley field appear to plot along the CO<sub>2</sub> reduction trend (Fig. 6A); however,  $\delta^{13}C$  values of CO<sub>2</sub> and CH<sub>4</sub> in the McCracken Formation (Fig. 6B) and low CO<sub>2</sub> concentrations in the Honaker Trail Formation are inconsistent with microbial methanogenesis (Whiticar et al., 1986; Martini et al., 1996; 2003; Vinson et al., 2019).

As the shallow reservoirs above the Paradox Formation source rocks

were brought closer to the surface by recent (<4–10 Ma) denudation of the Colorado Plateau and reached lower temperatures (<~80 °C; Nuccio and Condon, 1996; Rasmussen and Rasmussen, 2009) in contact with circulating meteoric waters (Kim et al., 2022a, 2022b; Tyne et al., 2022), microbial communities may have been re-introduced into previously sterilized reservoirs (Head et al. 2003), stimulating biodegradation of hydrocarbons and microbial methanogenesis (Fig. 9B and 9C). In particular, the further northeastern fields – Andy's Mesa, Hamilton Creek, and Cisco fields – are proximal to the Uncompahgre Uplift topographic high and regional discharge areas (e.g., Colorado River). This topography and associated hydraulic gradients promote greater meteoric fluxes and may enhance microbial activity in the shallow reservoirs (Fig. 9C) (McIntosh et al., 2023). The dissolution of gypsum by meteoric circulation around salt walls and related anticlines (Kim et al.,

2022a) could have promoted BSR and anaerobic oxidation of hydrocarbons as seen in other sedimentary basins (Adams et al., 2013; Bose et al., 2013) (Fig. 9B). Consumption of sulfate by BSR or paucity of sulfate sources, away from salt walls, may have promoted microbial methanogenesis in organic-rich reservoirs. Microbial methane in the Dakota and Morrison formations may have been generated from biodegradation of in situ carbonaceous materials, crude oil, and/or thermogenic gases (Pallasser, 2000). The extent and mechanism of microbial processes in these shallow hydrocarbon reservoirs, related to fluxes of electron acceptors (e.g., SO<sub>4</sub>), are the focus of future work.

#### 5.5. Alternative sources of CO2

It is notable that the Leadville and McCracken formations contain high CO<sub>2</sub> concentrations (1–48 mol%; Table 1) with a narrow range of  $\delta^{13}C_{CO2}$  (-7.5  $\pm$  0.7%; Table 2) relative to other formations. Their δ<sup>13</sup>C<sub>CO2</sub> values are within a plausible range of thermogenic gases from approximately -40 to +10% (Milkov and Etiope, 2018), but are also similar to mantle-sourced  $CO_2$  in the region (-7.0 to -3.5%; Crossey et al., 2009; Craddock et al., 2017). This suggests an influx of abiotic CO<sub>2</sub> into the Leadville and McCracken formations through the Precambrian basement or Cenozoic volcanic rocks (e.g., La Sal Mountains). Although there is no evidence of abiotic methane in the basal formations in either the conventional gas isotope signatures (Figs. 3 and 5C) or  $\Delta^{13}$ CH<sub>3</sub>D values (Fig. 7A). CO<sub>2</sub> and other crustal- or magmatic-derived gases (i.e., basement <sup>4</sup>He flux) have accumulated in the basal hydrostratigraphic units, sealed by overlying Paradox Formation evaporite confining units (Tyne et al., 2022). Alternatively, decarboxylation of the Leadville Formation carbonate rocks (Crossey et al., 2009) and/or microbial degradation of hydrocarbons, possibly promoted by influx of meteoric water and cooler temperatures following denudation (Kim et al., 2022b), could have contributed CO2.

# 5.6. Temporal evolution of $\Delta^{13}$ CH<sub>3</sub>D and $\varepsilon_{methane/water}$ values

Consideration of how  $\Delta^{13}$ CH<sub>3</sub>D values evolve through geologic time, in response to deep burial and higher temperatures versus uplift/ denudation and cooling (Fig. 8), and exchange rates of hydrogen isotopes between methane and water, provides further insights into clumped isotope signatures of natural gas. According to Turner et al. (2022), the timescale for  $\Delta^{13}$ CH<sub>3</sub>D exchange (1/k) is ~5.4 m.y. at 160 °C and 100 m.y. at 110  $^{\circ}$ C. The Cane Creek source rocks in the northeastern part of the basin experienced the maximum temperature of up to 160 °C over 40 m.y., whereas the Ismay-Desert Creek source rocks in the southwestern part of the basin were heated to below 110 °C over 50 m.y. (Fig. 2). Thus, methane within the source rocks in the northeastern side of the basin (e.g., Lisbon Valley field) should have been thermally reequilibrated, whereas methane in the southwestern side of the basin (e.g., Greater Aneth field) would have retained the original clumped isotope signals. Therefore, we interpret that  $\Delta^{13}$ CH<sub>3</sub>D values of 2.5 to 3.0% ( $T_{13D} = 160$  to 200 °C; Table 2) measured in reservoirs above the Paradox Formation source rocks in the northeastern fields represent thermal equilibrium during maximum burial. Conversely, the low  $\Delta^{13}$ CH<sub>3</sub>D values measured in the Paradox Formation gases (0.3 and 0.9%, Table 2) in the Greater Aneth field and Leadville/McCracken formation gases (1.3–2.1‰) indicate the preservation of kinetic signals from initial thermal cracking of organic matter. Note that the actual equilibrium curve for natural methane at the condition of each reservoir can differ from the gas-phase equilibrium curve predicted by theory and calibrated in the laboratory (Xie et al., 2021).

 $\Delta^{13} CH_3D$  and  $\epsilon_{methane/water}$  equilibrium is achieved at temperatures above 160 °C in the model, according to Eq. (2) and Eq. (3). Thus, once methane is equilibrated with  $\Delta^{13} CH_3D$  and hydrogen isotopes of water, the final  $\Delta^{13} CH_3D$  and  $\epsilon_{methane/water}$  values reflect the environmental conditions of the last equilibrium, regardless of any choice of initial  $\Delta^{13} CH_3D$  and  $\epsilon_{methane/water}$  values. In the model of the source rocks

(Cane Creek members of the Paradox Formation) in the Lisbon Valley field, the mean values of measured  $\Delta^{13} CH_3 D$  and  $\epsilon_{methane/water}$  values were used as initial values. The thermally equilibrated  $\Delta^{13} CH_3 D$  (Fig. 8A) is consistent with the high thermal maturities of the source rocks (Fig. 1B) and hydrocarbons remaining in the reservoirs above and below the Paradox Formation (Figs. 3 and 5C). This observation suggests that thermogenic gases containing thermally equilibrated  $\Delta^{13} CH_3 D$  represent hydrocarbons from a source that reached high thermal maturity.

The mature thermogenic gases, with  $\Delta^{13} \text{CH}_3 \text{D}$  values corresponding to equilibration at 160–170 °C over  $\sim\!50$  m.y. (30–80 Ma; Fig. 8A), would have been expelled into the overlying Honaker Trail Formation reservoirs during maximum burial, along faults (Fig. 9B). The relatively early generated, low to moderate maturity thermogenic gases that migrated during the beginning stage of burial (80–100 Ma) into the underlying Leadville/McCracken formations, would have not been equilibrated with respect to  $\Delta^{13} \text{CH}_3 \text{D}$  with unreasonably high  $T_{13D}$  values (247–374 °C) compared to the burial/thermal history of the basal formations (<200 °C; Fig. 2A). Although the modeled  $\Delta^{13} \text{CH}_3 \text{D}$ -based temperature at equilibrium slightly decreased from 170 to 160 °C between 30 Ma to the present due to cooling effects (by uplift and erosion) (Fig. 8A),  $\Delta^{13} \text{CH}_3 \text{D}$  values still closely reflect the equilibrium temperature of the last deep burial.

The modeled  $\epsilon_{methane/water}$  values for the Lisbon Valley field, based on the thermal histories, suggest methane resided at depth under relatively high temperatures ( $\geq 160~^{\circ}$ C) for enough time (e.g., at least for 40 m.y. between 30 and 70 Ma; Fig. 8A) for hydrogen isotope exchange of hydrocarbons with formation water (Koepp, 1978; Sessions et al., 2004; Xie et al., 2020 & 2021). It is also possible that methane has (re)equilibrated with some other sources of hydrogen such as  $H_2$  (0.5 mol% from the Leadville/McCracken formations; Table 1) and other hydrogenbearing compounds (e.g., on clay mineral surfaces) or that the hydrogen (D/H) exchange responsible for the (re)equilibrium has been accelerated by interaction with catalytic materials, such as metal oxide and organometallic complexes (Sattler, 2018; Giunta et al., 2021).

If we assume the thermal history of the Cutler Group and Honaker Trail Formation in the Andy's Mesa and Hamilton Creek fields is similar to the nearby Lisbon Valley (Fig. 2A), deep burial of the source rocks in the northeastern part of the basin above 160 °C would have led to  $\Delta^{13}\mathrm{CH_3D}$  equilibrium (Fig. 8A) with measured  $T_{13D}$  values of 160–195 °C. Later AOM, following denudation, would have led to disequilibrium in  $\Delta^{13}\mathrm{CH_3D}$  and hydrogen isotopes between CH<sub>4</sub> and H<sub>2</sub>O, as observed at present. There might also have not been enough time for recent recharge waters, with lower  $\delta D_{\mathrm{H2O}}$  values, to have equilibrated with methane (Kim et al., 2022b).

The high  $\Delta^{13}$ CH<sub>3</sub>D value (5.2‰) of one sample (HC12-13) from the Honaker Trail Formation in the Hamilton Creek field, plotting in the mixed microbial-thermogenic gas field (Fig. 7), is identical to the modeled  $\Delta^{13}CH_3D$  value in equilibrium at present temperature (Fig. 8A). This sample could have been affected by AOM or mixed with (secondary) microbial methane at low apparent temperatures ( $T_{13D}$  of 47 °C) following recent denudation. AOM can (re)equilibrate methane (Fig. 8A) through exchange catalysis during enzymatic back reactions (Ash et al., 2019) under low temperature (<70 °C) conditions. Interestingly, the bulk carbon isotopic composition of this sample shows no evidence of anaerobic oxidation (e.g., carbon isotopic reversal between  $CH_4$  and  $C_2$ ), indicating  $\Delta^{13}CH_3D$  may be a more sensitive tracer for microbial carbon cycling, as recently suggested by Giunta et al. (2022). Alternatively, the sample's  $\Delta^{13}CH_3D$  value plots within the range of abiotic methane (Wang et al., 2015; Young et al., 2017; Douglas et al., 2017), and its  $\delta^{13}C_{CO2}$  values (-7.1  $\pm$  0.2%; Table 2) are similar to mantle-sourced CO<sub>2</sub> in the region (Crossey et al., 2009; Craddock et al., 2017). As mentioned above, characterization of microbial communities in these hydrocarbon reservoirs is needed to further interpret methane isotopologue signatures.

In the models for the Greater Aneth field (Fig. 8B), because of the

lack of initial  $\Delta^{13} CH_3 D$  and  $\epsilon_{methane/water}$  data at 100 Ma, initial values were assumed to be similar to measured values of gases present today in the source rocks ( $\Delta^{13} CH_3 D$  of 0.3% and  $\epsilon_{methane/water}$  of -250%). The temperature during maximum burial ( $\leq \! 110$  °C) was too low to equilibrate  $\Delta^{13} CH_3 D$  and  $\epsilon_{methane/water}$  in the source rocks (i.e., Ismay-Desert Creek members of the Paradox Formation) (Fig. 8B). The modeled  $\Delta^{13} CH_3 D$  and  $\epsilon_{methane/water}$  values slightly increased during burial (25–80 Ma) without reaching equilibrium and then maintained their values after cooling. The observed disequilibration of  $\Delta^{13} CH_3 D$  and hydrogen isotopes between methane and water (Fig. 8B) supports the low thermal maturity of hydrocarbons in the Greater Aneth field.

In the three models for source rocks in the Cisco field (Fig. 8C), the average measured  $\Delta^{13}\text{CH}_3\text{D}$  (3.4%) and  $\epsilon_{methane/water}$  (–190%) values were used as initial values at 100 Ma. The forward model results particularly starting 140 °C, based on the thermal and burial history of the shallow source rocks in the field (Figs. 2C and 9C), align with measured  $\Delta^{13}\text{CH}_3\text{D}$  and  $\epsilon_{methane/water}$  values. This observation suggests that high  $\Delta^{13}$ CH<sub>3</sub>D values, corresponding to the low range of  $T_{13D}$  values (133  $\pm$  27 °C), can be explained by multiple mechanisms for methane generation. Thermogenic methane first equilibrated with  $\Delta^{13}$ CH<sub>3</sub>D under high temperature (130-140 °C) conditions around 60-100 Ma, while secondary microbial methane was generated more recently (around 10-50 Ma), possibly from oil biodegradation, and equilibrated with δD of water under lower temperatures (20-40 °C) (Figs. 7B, 8C, and 9C) (Head et al., 2003; Wang et al., 2015). The new equilibrium model, based on the hydrogen isotope exchange rate and thermal history, helps constrain methane isotopologue signatures and the temporal evolution of hydrocarbons in the subsurface.

#### 6. Conclusions

Results of this study highlight the applicability of clumped isotopologues ( $\Delta^{13} \text{CH}_3 \text{D}$ ) to illuminate veiled isotopic signals of microbial methane, obfuscated by the presence of thermogenic gas and anaerobic oxidation of hydrocarbons. Furthermore, this study constructed a new equilibrium model based on the hydrogen isotope exchange rate between CH<sub>4</sub> and H<sub>2</sub>O and basin thermal history to support the temporal evolution of  $\Delta^{13} \text{CH}_3 \text{D}$  values – a new approach in hydrocarbon geochemistry. The integrated observation and modeling results, including conventional and clumped isotopes, provides a better understanding of the origins and fate of hydrocarbons in dynamic and complex shallow crustal environments.

The pervasive presence of thermogenic gases, in reservoirs above and below the Paradox Formation shale source rocks, in the Paradox Basin is consistent with the basin's deep burial history. Biodegradation of hydrocarbons and presence of microbial methane points to recent denudation and meteoric circulation enhancing microbial activity in shallow reservoirs.

[1] Low-maturity thermogenic gases are present along the southwestern margin of the basin that was never deeply buried. The low  $\Delta^{13}\text{CH}_3\text{D}$  values of these thermogenic gases suggest methane retained its disequilibrium signal from initial generation.

[2] Low to moderate maturity thermogenic gases were generated in Paradox Formation source rocks, interbedded with evaporites, during early burial of the northeastern part of the basin, and expelled into underlying reservoirs, trapped by the salt walls. As the basin continued to subside, methane in the underlying reservoirs was isolated from the source rocks and thermally disequilibrated with respect to  $\Delta^{13} \text{CH}_3 \text{D}$ . During maximum burial, higher maturity hydrocarbons were generated in the Paradox Formation source rocks and expelled into overlying reservoirs, and later biodegraded via anaerobic oxidation of hydrocarbons, especially ethane and propane. The biodegradation of hydrocarbons was likely enhanced by recent denudation of the Colorado Plateau in the last  $\sim\!4$ –10 Ma and coupled to BSR with abundant sulfate from meteoric circulation and

gypsum dissolution around salt walls. Microbial methane, isotopically equilibrated with water, was also generated in the shallowest oil/gas reservoirs and mixed with thermogenic gases.

[3] The  $\Delta^{13}CH_3D$  and hydrogen isotopic equilibrium results in this study provide new insights for a dichotomy of disequilibrium between low-maturity thermogenic gases and biodegraded thermally-mature thermogenic gases. Study results also extend the field of  $\Delta^{13}CH_3D$  values of thermogenic gases. Together with more traditional molecular and isotopic gas composition,  $\Delta^{13}CH_3D$  is a sensitive tracer for illuminating the history of carbon cycling in sedimentary basins from initial generation of hydrocarbons, maximum burial and thermal equilibration, and post-genetic biodegradation, following denudation and meteoric circulation.

#### **Declaration of Competing Interest**

The authors declare that they have no known competing financial interests or personal relationships that could have appeared to influence the work reported in this paper.

#### Acknowledgements

Funding for this research was provided by the W.M. Keck Foundation, CIFAR, and NSF EAR SMRFS project (#2120733). McIntosh is a fellow of the CIFAR Earth4D Subsurface Science and Exploration program. The authors would like to acknowledge Paradox Resources, Navajo Nation Oil and Gas Company, and Running Foxes Petroleum for help with sampling. Paradox Resources also provided unpublished data for comparison. The authors also acknowledge Jackson Watkins, Dr. Bradley Stevenson, and Dr. Magdalena Osburn at Northwestern University for help with sampling. Dr. Jon Thorson provided insights on petroleum systems in the Paradox Basin. In addition, the Canada First Research Excellence Fund and Korea Institute of Geoscience and Mineral Resources (KIGAM) (GP2020-006) partially supported this research. Three anonymous reviewers provided constructive comments that greatly improved the manuscript.

# Appendix A. Supplementary material

Research data associated with the forward models for  $\Delta^{13}CH_3D$  equilibration are available in the Supplementary Material and include time, temperature of source rocks, equilibrium temperature based on modeled  $\Delta^{13}CH_3D$ , modeled  $\Delta^{13}CH_3D$  values,  $\Delta^{13}CH_3D$  values expected from equilibrium, modeled  $\epsilon_{methane/water}$  values, and  $\epsilon_{methane/water}$  values expected from equilibrium for Lisbon Valley, Greater Aneth, and Cisco fields. The dataset of the Cisco field consists of three different results depending on the initial temperatures of source rocks ( $T_0=160,\,140,\,110\,^{\circ}C$ ). Supplementary material to this article can be found online at https://doi.org/10.1016/j.gca.2023.10.017.

# References

Adams, M.M., Hoarfrost, A.L., Bose, A., Joye, S.B., Girguis, P.R., 2013. Anaerobic oxidation of short-chain alkanes in hydrothermal sediments: potential influences on sulfur cycling and microbial diversity. Front. Microbiol. 4, 110.

Ash, J.L., Egger, M., Treude, T., Kohl, I., Cragg, B., Parkes, R.J., Slomp, C.P., Sherwood Lollar, B., Young, E.D., 2019. Exchange catalysis during anaerobic methanotrophy revealed by <sup>12</sup>CH<sub>2</sub>D<sub>2</sub> and <sup>13</sup>CH<sub>3</sub>D in methane. Geochem. Persp. Let. 10, 26–30.

Baars, D.L., 1966. Pre-Pennsylvanian paleotectonics—Key to basin evolution and petroleum occurrences in Paradox Basin, Utah and Colorado. Am. Assoc. Pet. Geol. Bull. 50, 2082–2111.

Baars, D.L., Stevenson, G.M., 1982. Subtle stratigraphic traps in Paleozoic rocks of Paradox basin. In: Halbouty, M.T. (Ed.), The Deliberate Search for the Subtle, vol. 32. Trap. Am. Assoc. Pet. Geol. Mem., pp. 131–158

Bailey, L.R., Drake, H., Whitehouse, M.J., Reiners, P.W., 2022a. Characteristics and consequences of red bed bleaching by hydrocarbon migration: A natural example from the Entrada sandstone, southern Utah. Geochem. Geophys. Geosystems. 23.

Bailey, L.R., Kirk, J., Hemming, S.R., Krantz, R.W., Reiners, P.W., 2022b. Eocene fault-controlled fluid flow and mineralization in the Paradox Basin, United States. Geology 50, 326–330.

- Barbeau, D.L., 2003. A flexural model for the Paradox Basin: implications for the tectonics of the Ancestral Rocky Mountains. Basin Res. 15, 97–115.
- Barton, M.D., Barton, I., Thorson, J., 2018. Paleofluid Flow in the Paradox Basin: Introduction. Soc. Econ. Geol. Guidebook Series 59, 1–12.
- Beaudry, P., Stefánsson, A., Fiebig, J., Rhim, J.H., Ono, S., 2021. High temperature generation and equilibration of methane in terrestrial geothermal systems: Evidence from clumped isotopologues. Geochim. Cosmochim. Acta 309, 209–234.
- Beitler, B., Chan, M.A., Parry, W.T., 2003. Bleaching of Jurassic Navajo Sandstone on Colorado Plateau Laramide highs: evidence of exhumed hydrocarbon supergiants? Geology 31, 1041–1044.
- Bernard, B.B., Brooks, J.M., Sackett, W.M., 1976. Natural gas seepage in the Gulf of Mexico. Earth Planet. Sci. Lett. 31, 48–54.
- Bose, A., Rogers, D.R., Adams, M.M., Joye, S.B., Girguis, P.R., 2013. Geomicrobiological linkages between short-chain alkane consumption and sulfate reduction rates in seep sediments. Front. Microbiol. 4, 386.
- Burruss, R.C., Laughrey, C.D., 2010. Carbon and hydrogen isotopic reversals in deep basin gas: Evidence for limits to the stability of hydrocarbons. Org. Geochem. 41, 1285–1296.
- Cater, F.W., Craig, L.C., 1970. Geology of the salt anticline region in southwestern Colorado. U.S. Geol. Surv. Prof. Pap. 637, 80.
- Chan, M.A., Parry, W.T., Bowman, J.R., 2000. Diagenetic hematite and manganese oxides and fault-related fluid flow in Jurassic sandstones, southeastern Utah. Am. Assoc. Pet. Geol. Bull. 84, 1281–1310.
- Chung, H.M., Gormly, J.R., Squires, R.M., 1988. Origin of gaseous hydrocarbons in subsurface environments: theoretical considerations of carbon isotope distribution. Chem. Geol. 71, 97–104.
- Craddock, W.H., Blondes, M.S., DeVera, C.A., Hunt, A.G., 2017. Mantle and crustal gases of the Colorado Plateau: Geochemistry, sources, and migration pathways. Geochim. Cosmochim. Acta 213, 346–374.
- Crossey, L.J., Karlstrom, K.E., Springer, A.E., Newell, D., Hilton, D.R., Fischer, T., 2009. Degassing of mantle-derived CO<sub>2</sub> and He from springs in the southern Colorado Plateau region—Neotectonic connections and implications for groundwater systems. Geol. Soc. Am. Bull. 121, 1034–1053.
- Doelling, H.H., Oviatt, C.G., Huntoon, P.W., 1988. Geology of Salt Valley anticline and Arches National Park, Grand County, Utah. Salt deformation in the Paradox region, Utah. Utah Geol. Min. Surv. Bull. 122, 1–60.
- Douglas, P.M.J., Stolper, D.A., Smith, D.A., Anthony, K.W., Paull, C.K., Dallimore, S., Wik, M., Crill, P.M., Winterdahl, M., Eiler, J.M., Sessions, A.L., 2016. Diverse origins of Arctic and Subarctic methane point source emissions identified with multiplysubstituted isotopologues. Geochim. Cosmochim. Acta 188, 163–188.
- Douglas, P.M., Stolper, D.A., Eiler, J.M., Sessions, A.L., Lawson, M., Shuai, Y., Bishop, A., Podlaha, O.G., Ferreira, A.A., Neto, E.V.S., Niemann, M., 2017. Methane clumped isotopes: Progress and potential for a new isotopic tracer. Org. Geochem. 113, 262–282.
- Eldridge, D.L., Korol, R., Lloyd, M.K., Turner, A.C., Webb, M.A., Miller III, T.F., Stolper, D.A., 2019. Comparison of Experimental vs Theoretical Abundances of <sup>13</sup>CH<sub>3</sub>D and <sup>12</sup>CH<sub>2</sub>D<sub>2</sub> for Isotopically Equilibrated Systems from 1 to 500 °C. ACS Earth Space Chem. 3. 2747–2764.
- Foxford, K.A., Walsh, J.J., Watterson, J., Garden, I.R., Guscott, S.C., Burley, S.D., 1998. Structure and content of the Moab Fault Zone, Utah, USA, and its implications for fault seal prediction. Geolog. Soci. London, Special Publications 147, 87–103.
- Friedman, J.D., Huffman Jr, A.C., 1998. Laccolith complexes of southeastern Utah; time of emplacement and tectonic setting; workshop proceedings (No. 2158). USGPO; U. S. Geol. Surv. Information Services.
- Giunta, T., Young, E.D., Warr, O., Kohl, I., Ash, J.L., Martini, A., Mundle, S.O., Rumble, D., Pérez-Rodríguez, I., Wasley, M., LaRowe, D.E., 2019. Methane sources and sinks in continental sedimentary systems: New insights from paired clumped isotopologues <sup>13</sup>CH<sub>3</sub>D and <sup>12</sup>CH<sub>2</sub>D<sub>2</sub>. Geochim. Cosmochim. Acta 245, 327–351.
- Giunta, T., Labidi, J., Kohl, I.E., Ruffine, L., Donval, J.P., Géli, L., Çağatay, M.N., Lu, H., Young, E.D., 2021. Evidence for methane isotopic bond re-ordering in gas reservoirs sourcing cold seeps from the Sea of Marmara. Earth Planet. Sci. Lett. 553, 16619.
- Giunta, T., Young, E.D., Labidi, J., Sansjofre, P., Jézéquel, D., Donval, J.P., Brandily, C., Ruffine, L., 2022. Extreme methane clumped isotopologue bio-signatures of aerobic and anaerobic methanotrophy: Insights from the Lake Pavin and the Black Sea sediments. Geochim. Cosmochim. Acta 338, 34–53.
- Hahn, G.A., Thorson, J.P., 2006. Geology of the Lisbon Valley sandstone-hosted disseminated copper deposits, San Juan County, Utah. Utah Geol. Assoc. Publ. 32, 511–533
- 511–533. Hanshaw, B.B., Hill, G.A., 1969. Geochemistry and hydrodynamics of the Paradox basin
- region, Utah, Colorado and New Mexico. Chem. Geol. 4, 263–294. Hartley, A., Evenstar, L., 2018. Fluvial architecture in actively deforming salt basins: Chinle Formation, Paradox Basin, Utah. Basin Res. 30, 148–166.
- Head, I.M., Jones, D.M., Larter, S.R., 2003. Biological activity in the deep subsurface and the origin of heavy oil. Nature 426, 344–352.
- Hendel, C.W., 1961. Cisco Townsite Field, Grand County, Utah. Oil and Gas Fields of Utah: A Symposium.
- Hite, R.J., Anders, D.E., Ging, T.G., 1984. Organic-rich source rocks of Pennsylvanian age in the Paradox Basin of Utah and Colorado. In: Woodward, J., Meissner, F.F., Clayton, J.L. (Eds.), Hydrocarbon Source Rocks of the Greater Rocky Mountain Region. Rocky Mountain Association of Geologists, Denver, Colorado, pp. 255–274.
- Hodson, K.R., Crider, J.G., Huntington, K.W., 2016. Temperature and composition of carbonate cements record early structural control on cementation in a nascent deformation band fault zone: Moab Fault, Utah, USA. Tectonophysics 690, 240–252.
- Hoffman, M., 2009. Mio-Pliocene erosional exhumation of the central Colorado Plateau, eastern Utah: New insights from apatite (U-Th)/He thermochronometry (Doctoral dissertation, University of Kansas).

- James, A.T., Burns, B.J., 1984. Microbial alteration of subsurface natural gas accumulations. Am. Assoc. Pet. Geol. Bull. 68, 957–960.
- Jautzy, J.J., Douglas, P.M., Xie, H., Eiler, J.M., Clark, I.D., 2021. CH<sub>4</sub> isotopic ordering records ultra-slow hydrocarbon biodegradation in the deep subsurface. Earth Planet. Sci. Lett. 562, 116841.
- Jenden, P.D., Kaplan, I.R., 1989. Origin of natural gas in Sacramento Basin, California. Am. Assoc. Pet. Geol. Bull. 73, 431–453.
- Jones, D.M., Head, I.M., Gray, N.D., Adams, J.J., Rowan, A.K., Aitken, C.M., Bennett, B., Huang, H., Brown, A., Bowler, B.F.J., Oldenburg, T., 2008. Crude-oil biodegradation via methanogenesis in subsurface petroleum reservoirs. Nature 451, 176–180.
- Karlstrom, K.E., Coblentz, D., Dueker, K., Ouimet, W., Kirby, E., Van Wijk, J., Schmandt, B., Kelley, S., Lazear, G., Crossey, L.J., Crow, R., 2012. Mantle-driven dynamic uplift of the Rocky Mountains and Colorado Plateau and its surface response: Toward a unified hypothesis. Lithosphere 4, 3–22.
- Kim, J.H., Bailey, L., Noyes, C., Tyne, R.L., Ballentine, C.J., Person, M., Ma, L., Barton, M., Barton, I., Reiners, P.W., Ferguson, G., McIntosh, J., 2022a. Hydrogeochemical evolution of formation waters responsible for sandstone bleaching and ore mineralization in the Paradox Basin, Colorado Plateau, USA. Geol. Soc. Am. Bull. 134. 2589–2610.
- Kim, J.H., Ferguson, G., Person, M., Jiang, W., Lu, Z.T., Ritterbusch, F., Yang, G.M., Tyne, R., Bailey, L., Ballentine, C., Reiners, P., McIntosh, J., 2022b. Krypton-81 dating constrains timing of deep groundwater flow activation. Geophys. Res. Lett. 49
- King, V.M., Block, L.V., Yeck, W.L., Wood, C.K., Derouin, S.A., 2014. Geological structure of the Paradox Valley Region, Colorado, and relationship to seismicity induced by deep well injection. J. Geophys. Res. Solid Earth 119, 4955–4978.
- Knittel, K., Boetius, A., 2009. Anaerobic oxidation of methane: progress with an unknown process. Annu. Rev. Microbiol. 63, 311–334.
- Koepp, M., 1978. D/H isotope exchange reaction between petroleum and water: A contributory determinant for D/H-isotope ratios in crude oil?. In: Short Papers of the Fourth International Conference. Geochronology. Cosmochronology. Isotope Geology, 1978, 221–222. US Geological Survey.
- Lawton, T.F., Buller, C.D., Parr, T.R., 2015. Provenance of a Permian erg on the western margin of Pangea: Depositional system of the Kungurian (late Leonardian) Castle Valley and White Rim sandstones and subjacent Cutler Group, Paradox Basin, Utah, USA. Geosphere 11, 1475–1506.
- Lazear, G., Karlstrom, K., Aslan, A., Kelley, S., 2013. Denudation and flexural isostatic response of the Colorado Plateau and southern Rocky Mountains region since 10 Ma. Geosphere 9, 792–814.
- Leary, R.J., Umhoefer, P., Smith, M.E., Riggs, N., 2017. A three-sided orogen: A new tectonic model for Ancestral Rocky Mountain uplift and basin development. Geology 45, 735–738.
- Lorant, F., Prinzhofer, A., Behar, F., Huc, A.Y., 1998. Carbon isotopic and molecular constraints on the formation and the expulsion of thermogenic hydrocarbon gases. Chem. Geol. 147, 249–264.
- Lucero, D., Bailey, L., Person, M., Hughes, A., Krantz, R.W., Lingrey, S., Barton, M., Reiners, P.W., McIntosh, J.C., Neuzil, C., Thorson, J.P., 2020. Influence of internal fluid generation mechanisms on redbed alteration in the Paradox Basin, Utah. Geological Society of America 2020 Connects Online, https://doi.org/10.1130/ /abs/2020AM-358545
- Ma, Q., Wu, S., Tang, Y., 2008. Formation and abundance of doubly-substituted methane isotopologues (13CH3D) in natural gas systems. Geochim. Cosmochim. Acta. 72, 5446–5456.
- Martini, A.M., Budai, J.M., Walter, L.M., Prinzhofer, M., 1996. Microbial generation of economic accumulations of methane within a shallow organic-rich shale. Nature 383 155–158
- Martini, A.M., Walter, L.M., Budai, J.M., Ku, T.C., Kaiser, C.J., Schoell, M., 1998. Genetic and temporal relations between formation waters and biogenic methane: Upper Devonian Antrim Shale, Michigan Basin, USA. Geochim. Cosmochim. Acta 62, 1699–1720.
- Martini, A.M., Walter, L.M., Ku, T.C., Budai, J.M., McIntosh, J.C., Schoell, M., 2003. Microbial production and modification of gases in sedimentary basins: A geochemical case study from a Devonian shale gas play, Michigan basin. Am. Assoc. Pet. Geol. Bull. 87, 1355–1375.
- Martini, A.M., Walter, L.M., McIntosh, J.C., 2008. Identification of microbial and thermogenic gas components from Upper Devonian black shale cores, Illinois and Michigan basins. Am. Assoc. Pet. Geol. Bull. 92, 327–339.
- Masterson, W.D., Dzou, L.I., Holba, A.G., Fincannon, A.L., Ellis, L., 2001. Evidence for biodegradation and evaporative fractionation in West Sak, Kuparuk and Prudhoe Bay field areas, North Slope, Alaska. Org. Geochem. 32, 411–441.
- Matyasik, I., Steczko, A., Philp, R.P., 2000. Biodegradation and migrational fractionation of oils from the Eastern Carpathians. Poland. Org. Geochem. 31, 1509–1523.
- McBride, E.F., 2016. Stratigraphy, petrography, and depositional history of the Ignacio Quartzite and McCracken Sandstone Member of the Elbert Formation, southwestern Colorado, USA. Rocky Mt. Geol. 51, 23–68.
- McIntosh, J.C., Hendry, M.J., Ballentine, C., Haszeldine, R.S., Mayer, B., Etiope, G., Elsner, M., Darrah, T.H., Prinzhofer, A., Osborn, S., Stalker, L., 2018. A critical review of state-of-the-art and emerging approaches to identify fracking-derived gases and associated contaminants in aquifers. Environ. Sci. Technol. 53, 1063–1077.
- McIntosh, J., Kim, J.H., Bailey, L., Osburn, M., Drake, H., Martini, A., Reiners, P., Stevenson, B., Ferguson, G., 2023. Burial and Denudation Alter Microbial Life at the Bottom of the Hypo-Critical Zone. Geochem. Geophys. Geosystems. 24.
- Merin, I.S., Segal, D.B., 1989. Diagenetic alteration of the Wingate Formation: Possible indications of hydrocarbon microseepage, Lisbon Valley, Utah. J. Geol. 97, 719–734.
   Milkov, A.V., Etiope, G., 2018. Revised genetic diagrams for natural gases based on a
- global dataset of> 20,000 samples. Org. Geochem. 125, 109-120.

- Murray, K.E., Reiners, P.W., Thomson, S.N., 2016. Rapid Pliocene-Pleistocene erosion of the central Colorado Plateau documented by apatite thermochronology from the Henry Mountains. Geology 44, 483–486.
- Murray, K.E., Reiners, P.W., Thomson, S.N., Robert, X., Whipple, K.X., 2019. The thermochronologic record of erosion and magmatism in the Canyonlands region of the Colorado Plateau. Am. J. Sci. 319, 339–380.
- Nuccio, V.F., Condon, S.M., 1996. Burial and thermal history of the Paradox Basin, Utah and Colorado, and petroleum potential of the middle Pennsylvanian Paradox Formation. U.S. Geol. Surv. Bull. 2000-O.
- Ono, S., Wang, D.T., Gruen, D.S., Sherwood Lollar, B., Zahniser, M.S., McManus, B.J., Nelson, D.D., 2014. Measurement of a doubly substituted methane isotopologue, <sup>13</sup>CH<sub>3</sub>D, by tunable infrared laser direct absorption spectroscopy. Anal. Chem. 86, 6487–6494
- Osborn, S.G., McIntosh, J.C., 2010. Chemical and isotopic tracers of the contribution of microbial gas in Devonian organic-rich shales and reservoir sandstones, northern Appalachian Basin. Appl. Geochem. 25, 456–471.
- Pallasser, R.J., 2000. Recognising biodegradation in gas/oil accumulations through the δ<sup>13</sup>C compositions of gas components. Org. Geochem. 31, 1363–1373.
- Pederson, J., Burnside, N., Shipton, Z., Rittenour, T., 2013. Rapid river incision across an inactive fault—Implications for patterns of erosion and deformation in the central Colorado Plateau. Lithosphere 5, 513–520.
- Prinzhofer, A., Battani, A., 2003. Gas isotopes tracing: an important tool for hydrocarbons exploration. Oil Gas Sci. Technol. 58, 299–311.
- Prinzhofer, A.A., Huc, A.Y., 1995. Genetic and post-genetic molecular and isotopic fractionations in natural gases. Chem. Geol. 126, 281–290.
- Prinzhofer, A., Pernaton, E., 1997. Isotopically light methane in natural gas: bacterial imprint or diffusive fractionation? Chem. Geol. 142, 193–200.
- Rasmussen, L., Rasmussen, D.L., 2009. Burial history analysis of the Pennsylvanian petroleum system in the deep Paradox Basin fold and fault belt, Colorado and Utah.
- Rice, C.A., 2003. Production waters associated with the Ferron coalbed methane fields, central Utah: chemical and isotopic composition and volumes. Int. J. Coal Geol. 56, 141–169.
- Rooney, M.A., Claypool, G.E., Chung, H.M., 1995. Modeling thermogenic gas generation using carbon isotope ratios of natural gas hydrocarbons. Chem. Geol. 126, 219–232. Sattler, A., 2018. Hydrogen/deuterium (H/D) exchange catalysis in alkanes. ACS Catal.
- Sattler, A., 2018. Hydrogen/deuterium (H/D) exchange catalysis in alkanes. ACS Catal. 8, 2296–2312.
  Schoell, M., 1988. Multiple origins of methane in the Earth. Chem. Geol. 71 (1–3), 1–10.
- Schweitzer, H., Ritter, D., McIntosh, J., Barnhart, E., Cunningham, A.B., Vinson, D., Orem, W., Fields, M.W., 2019. Changes in microbial communities and associated water and gas geochemistry across a sulfate gradient in coal beds: Powder River Basin, USA. Geochim. Cosmochim. Acta 245, 495–513.
- Sessions, A.L., Sylva, S.P., Summons, R.E., Hayes, J.M., 2004. Isotopic exchange of carbon-bound hydrogen over geologic timescales. Geochim. Cosmochim. Acta. 68, 1545–1559.
- Shuai, Y., Douglas, P.M., Zhang, S., Stolper, D.A., Ellis, G.S., Lawson, M., Lewan, M.D., Formolo, M., Mi, J., He, K., Hu, G., 2018. Equilibrium and non-equilibrium controls on the abundances of clumped isotopologues of methane during thermogenic formation in laboratory experiments: Implications for the chemistry of pyrolysis and the origins of natural gases. Geochim. Cosmochim. Acta 223, 159–174.
- Smouse, D., 1996. Greater Cisco Area: T. 19-21 S., R. 20-25 E., SLB&M: Grand County, Utah. Oil and Gas Fields of Utah.
- Stevenson, G.M., Baars, D.L., 1985. Paradox—Pull-Apart Basin of Pennsylvanian Age. Am. Assoc. Pet. Geol. Bull. 69, 867–868.
- Stolper, D.A., Lawson, M., Davis, C.L., Ferreira, A.A., Neto, E.S., Ellis, G.S., Lewan, M.D., Martini, A.M., Tang, Y., Schoell, M., Sessions, A.L., 2014a. Formation temperatures of thermogenic and biogenic methane. Science 344, 1500–1503.
- Stolper, D.A., Sessions, A.L., Ferreira, A.A., Neto, E.S., Schimmelmann, A., Shusta, S.S., Valentine, D.L., Eiler, J.M., 2014b. Combined <sup>13</sup>C–D and D-D clumping in methane: Methods and preliminary results. Geochim. Cosmochim. Acta 126, 169–191.
- Stolper, D.A., Martini, A.M., Clog, M., Douglas, P.M., Shusta, S.S., Valentine, D.L., Sessions, A.L., Eiler, J.M., 2015. Distinguishing and understanding thermogenic and biogenic sources of methane using multiply substituted isotopologues. Geochim. Cosmochim. Acta 161, 219–247.
- Stolper, D.A., Lawson, M., Formolo, M.J., Davis, C.L., Douglas, P.M., Eiler, J.M., 2018. The utility of methane clumped isotopes to constrain the origins of methane in natural gas accumulations. Geol. Soc. London, Special Publ. 468, 23–52.
- Thackston, J.W., McCulley, B.L., Preslo, L.M., 1981. Ground-water circulation in the western Paradox Basin, Utah. In: Wiegand, D.L. (Ed.), Geology of the Paradox basin. Rocky Mountain Association of Geologists Field Conference, pp. 201–225.
- Thorson, J.P., 2018. Paradox Basin fluids and Colorado Plateau copper, uranium, and vanadium deposits: Overview. Soc. Econ. Geol. Guidebook Series 59, 13–46.
- Thorson, J.P., MacIntyre, T.J., 2005. Geology of the Cashin Mine sandstone-hosted disseminated copper deposit, Montrose County, Colorado. Soc. Econ. Geol. Guidebook Series 37, 43–49.
- Tilley, B., Muehlenbachs, K., 2006. Gas maturity and alteration systematics across the Western Canada Sedimentary Basin from four mud gas isotope depth profiles. Org. Geochem. 37, 1857–1868.
- Trudgill, B.D., 2011. Evolution of salt structures in the northern Paradox Basin: Controls on evaporite deposition, salt wall growth and supra-salt stratigraphic architecture. Basin Res. 23, 208–238.

- Tsuji, K., Teshima, H., Sasada, H., Yoshida, N., 2012. Spectroscopic isotope ratio measurement of doubly-substituted methane. Spectrochim. Acta A Mol. Biomol. Spectrosc. 98, 43–46.
- Turner, A.C., Korol, R., Eldridge, D.L., Bill, M., Conrad, M.E., Miller III, T.F., Stolper, D. A., 2021. Experimental and theoretical determinations of hydrogen isotopic equilibrium in the system CH<sub>4</sub>H<sub>2</sub>H<sub>2</sub>O from 3 to 200 °C. Geochim. Cosmochim. Acta. 314, 223–269.
- Turner, A.C., Pester, N.J., Bill, M., Conrad, M.E., Knauss, K.G., Stolper, D.A., 2022. Experimental determination of hydrogen isotope exchange rates between methane and water under hydrothermal conditions. Geochim. Cosmochim. Acta. 329, 231–255
- Tyne, R.L., Barry, P.H., Cheng, A., Hillegonds, D.J., Kim, J.H., McIntosh, J.C., Ballentine, C.J., 2022. Basin architecture controls on the chemical evolution and <sup>4</sup>He distribution of groundwater in the Paradox Basin. Earth Planet. Sci. Lett. 589, 117580
- Valentine, D.L., 2011. Emerging topics in marine methane biogeochemistry. Annu. Rev. Mar. Sci. 3, 147–171.
- Vandré, C., Cramer, B., Gerling, P., Winsemann, J., 2007. Natural gas formation in the western Nile delta (Eastern Mediterranean): Thermogenic versus microbial. Org. Geochem. 38, 523–539.
- Vinson, D.S., Blair, N.E., Martini, A.M., Larter, S., Orem, W.H., McIntosh, J.C., 2017.
  Microbial methane from in situ biodegradation of coal and shale: A review and reevaluation of hydrogen and carbon isotope signatures. Chem. Geol. 453, 128–145.
- Vinson, D.S., Blair, N.E., Ritter, D.J., Martini, A.M., McIntosh, J.C., 2019. Carbon mass balance, isotopic tracers of biogenic methane, and the role of acetate in coal beds: Powder River Basin (USA). Chem. Geol. 530, 119329.
- Walton, P.T., 1956. Structure of the north Salt Valley-Cisco area, Grand County, Utah. Geology and Economic Deposits of East Central Utah, Seventh Annual Field Conference, 186–189.
- Wang, D.T., Gruen, D.S., Lollar, B.S., Hinrichs, K.U., Stewart, L.C., Holden, J.F., Hristov, A.N., Pohlman, J.W., Morrill, P.L., Könneke, M., Delwiche, K.B., 2015. Nonequilibrium clumped isotope signals in microbial methane. Science 348, 428-431.
- Wang, D.T., Welander, P.V., Ono, S., 2016. Fractionation of the methane isotopologues <sup>13</sup>CH<sub>4</sub>, <sup>12</sup>CH<sub>3</sub>D, and <sup>13</sup>CH<sub>3</sub>D during aerobic oxidation of methane by Methylococcus capsulatus (Bath). Geochim. Cosmochim. Acta 192, 186–202.
- Wang, W.C., Zhang, L.Y., Liu, W.H., Kang, Y., Ren, J.H., 2005. Effects of biodegradation on the carbon isotopic composition of natural gas—A case study in the bamianhe oil field of the Jiyang Depression, Eastern China. Geochem. J. 39, 301–309.
- Wenger, L.M., Davis, C.L., Isaksen, G.H., 2002. Multiple controls on petroleum biodegradation and impact on oil quality. SPE Reserv. Eval. Eng. 5, 375–383.
- Whidden, K.J., Lillis, P.G., Anna, L.O., Pearson, K.M., Dubiel, R.F., 2014. Geology and total petroleum systems of the Paradox Basin, Utah, Colorado, New Mexico, and Arizona.
- Whiticar, M.J., 1999. Carbon and hydrogen isotope systematics of bacterial formation and oxidation of methane. Chem. Geol. 161, 291–314.
- Whiticar, M.J., Faber, E., Schoell, M., 1986. Biogenic methane formation in marine and freshwater environments: CO<sub>2</sub> reduction vs. acetate fermentation—isotope evidence. Geochim. Cosmochim. Acta 50, 693–709.
- Geochim. Cosmochim. Acta 50, 693–709.

  Wilhelms, A., Larter, S.R., Head, I., Farrimond, P., di-Primio, R., Zwach, C., 2001.

  Biodegradation of oil in uplifted basins prevented by deep-burial sterilization.

  Nature 411, 1034–1037.
- Xia, X., Gao, Y., 2019. Kinetic clumped isotope fractionation during the thermal generation and hydrogen exchange of methane. Geochim. Cosmochim. Acta 248, 252–273
- Xie, H., Ponton, C., Formolo, M.J., Lawson, M., Ellis, G.S., Lewan, M.D., Ferreira, A.A., Morais, E.T., Spigolon, A.L., Sessions, A.L., Eiler, J.M., 2020. Position-specific distribution of hydrogen isotopes in natural propane: Effects of thermal cracking, equilibration and biodegradation. Geochim. Cosmochim. Acta 290, 235–256.
- Xie, H., Dong, G., Formolo, M., Lawson, M., Liu, J., Cong, F., Mangenot, X., Shuai, Y., Ponton, C., Eiler, J., 2021. The evolution of intra-and inter-molecular isotope equilibria in natural gases with thermal maturation. Geochim. Cosmochim. Acta 307, 22–41.
- Young, R.G., 1983. Petroleum in northeastern Grand County, Utah. Grand Junction Geol. Soc. 1–7.
- Young, E.D., Kohl, I.E., Lollar, B.S., Etiope, G., Rumble Iii, D., Li, S., Haghnegahdar, M.A., Schauble, E.A., McCain, K.A., Foustoukos, D.I., Sutclife, C., 2017. The relative abundances of resolved <sup>12</sup>CH<sub>2</sub>D<sub>2</sub> and <sup>13</sup>CH<sub>3</sub>D and mechanisms controlling isotopic bond ordering in abiotic and biotic methane gases. Geochim. Cosmochim. Acta 203, 235–264.
- Zhang, Y., Gable, C.W., Zyvoloski, G.A., Walter, L.M., 2009. Hydrogeochemistry and gas compositions of the Uinta Basin: A regional-scale overview. Am. Assoc. Pet. Geol. Bull. 98, 1087–1118.
- Zhi, D., Song, Y., Zheng, M., Qin, Z., Gong, D., 2021. Genetic types, origins, and accumulation process of natural gas from the southwestern Junggar Basin: New implications for natural gas exploration potential. Mar. Pet. Geol. 123, 104727.
- Zhou, Ś., Huang, H., Liu, Y., 2008. Biodegradation and origin of oil sands in the Western Canada Sedimentary Basin. Pet. Sci. 5, 87–94.